M 2020

U.PORTO
FEUP FACULDADE DE ENGENHARIA
UNIVERSIDADE DO PORTO

Fraunhofer
IWS

INVESTIGATION OF THE PROCESS WINDOW FOR LASER SURFACE HARDENING A SAE M2 HIGH-SPEED STEEL

FRANCISCO JORGE CARNEIRO MOREIRA DA SILVA

MASTER THESIS DISSERTATION

Mestrado Integrado em Engenharia Metalúrgica e de Materiais

Internal Supervisor: Elsa Wellenkamp de Sequeiros, Dr.-Ing

External Supervisor: Marko Seifert, Dipl.-Phys

September 25th, 2020

CANDIDATO	Francisco Jorge Carneiro Moreira da Silva	*CÓDIGO*	201503073
TÍTULO	Investigation of the Process Window for Laser Surface Hardening a SAE M2 High-speed steel		
DATA	12 de Outubro de 2020		
HORA	14h30		
JÚRI	*Presidente* Laura Maria Melo Ribeiro		DEMM/FEUP
	Arguente Ana Rosanete Lourenço Reis		DEMec/FEUP
	Orientador Elsa Wellenkamp de Sequeiros		DEMM/FEUP

“The first step is to establish that something is possible;
then probability will occur.”

Elon Musk

Abstract

The integration of laser surface hardening methodologies in the universe of high-speed steels, more specifically the SAE M2, aims to the acquisition of highly wear resistance components, with greater overall life span in service.

The present work had as main goal the definition of a viable process window for laser surface hardening a SAE M2. Annealed state and conventional hardened and tempered state SAE M2 were subjected to laser surface hardening. All the laser surface hardened specimens were subjected to a surface hardness and hardening depth analysis. Furthermore, for all the analyzed specimens a hardened layer was observed at the surface by optical microscopy. For the annealed base laser hardened material an interaction time of 16 seconds provided maximum surface hardness of 60 ± 1 HRC, and hardening depth of 0.8 mm. On the other and, the conventional hardened and tempered base laser hardened material presented maximum surface hardness of 69 ± 1 HRC, and hardening depth of 1.0 mm for an interaction time of 8 seconds. Microstructural analysis on the laser hardened specimens demonstrated the presence of three distinct microstructural zones: hardened zone, transition zone, and base material. Furthermore, MC and M_6C carbides were identified by XRD and analyzed by SEM/EDS on both base and laser hardened material. Lastly, a tempering evaluation was conducted after laser surface hardening. By comparison of the tempering curves, the annealed base laser surface hardened material presented similar behavior to the conventional heat treatment, where a surface hardness of 60 ± 1 HRC, at secondary hardening peak, was registered. The conventional hardened and tempered base laser surface hardened material presented a significant decrease of surface hardness, to around 64 ± 1 HRC at secondary hardening peak.

The combination of all the results suggests a relative high effectiveness of the laser surface hardening heat treatment and establishes a viable process window for future research.

Keywords

Laser Surface Hardening, High-speed Steel, SAE M2, DIN 1.3343

Resumo

A integração do endurecimento superficial por laser no universo dos aços rápidos, mais especificamente o SAE M2, visa a obtenção de componentes de elevada resistência ao desgaste, perspetivando um aumento do tempo de vida útil em serviço.

O presente trabalho teve como principal objetivo a definição de uma janela de processamento efetiva para o endurecimento superficial por laser do aço SAE M2. Foi testado material tanto no estado recozido assim como no estado revenido. Todas as amostras endurecidas por laser foram sujeitas a um estudo de dureza superficial e profundidade de endurecimento. Para todas, uma camada de endurecimento superficial foi observada por microscopia ótica. No caso do material de base no estado recozido, um tempo de interação de 16 segundos proporcionou uma dureza superficial máxima de 60 ± 1 HRC e uma profundidade de endurecimento máxima de 0,76 mm. Para o material de base no estado revenido, foram alcançados valores máximos de dureza superficial de 69 ± 1 HRC e de profundidade de endurecimento de 1,00 mm para um tempo de interação de 8 segundos. A análise microestrutural das amostras endurecidas por laser indicou a presença de três regiões microestruturais distintas: zona endurecida, zona de transição e material base. Além disso, foram identificados por XRD e analisados por SEM/EDS carbonetos MC e M_6C tanto em material de base como em material endurecido por laser. Por fim, foi ainda realizado um estudo do tratamento de revenido após endurecimento superficial por laser. Comparando as curvas de revenido, as amostras endurecidas por laser de material base no estado recozido apresentaram um comportamento semelhante ao tratamento térmico convencional, tendo sido registada uma dureza superficial de 60 ± 1 HRC no pico de endurecimento secundário. Por outro lado, o material base no estado revenido endurecido por laser apresentou uma diminuição significativa de dureza superficial, para 64 ± 1 HRC, no pico de endurecimento secundário.

A combinação de todos os resultados sugere uma elevada eficácia do tratamento térmico de endurecimento superficial por laser, assim como estabelece uma janela de processamento viável para futuro desenvolvimento.

Palavras-Chave

Endurecimento Superficial por Laser, Aços Rápidos, SAE M2, DIN 1.3343

Contents

List of Figures

List of Tables

Abbreviations

HSS	High-Speed Steel
SAE	Society of Automotive Engineers
HPDL	High Power Diode Laser
Nd:YAG	Neodymium-doped Yttrium Aluminum Garnet
HZ	Hardened Zone
TZ	Transition Zone
BM	Base Material
TEM	Transverse Electromagnetic Mode
FCC	Face-Centered Cubic
DSC	Differential Scanning Calorimetry
OM	Optical Microscopy
XRD	X-ray Diffraction
SEM	Scanning Electron Microscopy
EDS	Energy-dispersive X-ray spectroscopy

1. Introduction

The implementation of laser technology in the universe of materials processing has been achieved with great success since its introduction to industrial processes. More so, the development of laser technology in different industries is the result of a dynamic relationship where the system works on a push dynamic, when the technology is looking for a problem to solve, or on a pull dynamic, when industries are looking for a solution to a specific problem [1, 2]. Such success is not only due to the unparallel results that laser technology is capable of delivering, but also due to its unique characteristics as an industrial equipment, mainly its flexibility [1, 3, 4].

By applying a push strategy, in the field of laser surface hardening, the family of high-speed steels (HSS), particularly the SAE M2 presents itself as an excellent candidate to further improvement via laser processing. Such tool steel grade was developed to attend machining applications, characterized by high mechanical requests in extreme wear conditions. By merging the mechanical characteristics of the SAE M2 and the hardening potential of laser processing, it becomes evident that laser surface hardening such grade steel could enhance the overall performance during machining and cutting operations [5-7].

In literature [6, 8, 9] there are some examples of experiments of laser surface hardening a SAE M2, with favorable results in what regards the increase of hardness when compared to the conventional heat treatment, indicating possible increases in wear resistance. Apart from this, there isn't a detailed description of the microstructural changes, or even the extent of the increase in mechanical properties that laser surface hardening supports. For all these reasons, it is of the utmost interest to explore the potential of such technology in surface hardening a SAE M2, as well as identify and define accurate process parameters and understand their influence throughout the hardening process.

This thesis is then focused on laser surface hardening a SAE M2, aiming to obtain a hardened surface layer promoted by such heat treatment. The significant challenges to such research work are focused on the correct definition of the process parameters. These consent the definition of a viable process window for future research and allow for the understanding of their influence on the attributes of the

hardened layer, more specifically, surface hardness and hardening depth. The inherent complexity of the SAE M2 heat treatment is also a factor that strongly influences the assessment of the ideal laser operating conditions. Furthermore, two distinct initial microstructural states are considered during this study, annealed and conventional hardened and tempered states. It is possible to evaluate the potential impact of the initial microstructural state on the laser surface hardening process. Lastly, and considering the conventional heat treatment procedure and its metallurgical influences on the SAE M2, the posterior tempering heat treatment is also explored. The response to tempering by the laser surface hardened SAE M2 will provide information regarding possible variations in the tempering dynamics.

2. Literature Review

The current chapter serves as an introduction to the laser surface hardening subject and the SAE M2, along with the concepts involved in the merging of the two. Consequently, basic concepts of laser technology and its implementation on the process of surface hardening are described, followed by a broad description of the SAE M2, its microstructural and conventional heat treatment characteristics.

2.1. Basics of Laser Technology

The laser, acronym for light amplification by stimulated emission of radiation, is a device that emits light in the form of electromagnetic radiation through the process of stimulated emission, as predicted by Einstein in 1916 [10, 11]. Due to its unique properties and flexibility, laser technology is desirable to a broad spectrum of applications, capable of operating at excellent performance levels. Such characteristics are the high level of monochromacy, coherence, directionality, brightness, and short pulse duration [12].

To produce a useful laser beam, a laser system is built around three main components, this being, an active medium; a pumping source; and an optical resonator. The active medium is where the electromagnetic wave is generated by a process referred to as pumping; the pumping source is necessary to excite the active medium; and the optical resonator is responsible for creating an amplified laser beam [10, 13-15].

There are in existence a diverse number of industrial laser systems, each one presenting singular characteristics in what regards properties such as active medium, power output, wavelength, and operation mode. For laser surface hardening, three types of laser systems stand out due to their high energy delivery, needed for this kind of process: the carbon dioxide (CO_2) laser, the neodymium-doped yttrium aluminum garnet (Nd:YAG) laser, and the High-Power Diode Laser (HPDL) [1, 2, 16]. Over the past few decades, heat treatment operations with CO_2 and Nd:YAG lasers have been well established. More recently, the HPDL, or semiconductor laser, has gained recognition due to its higher efficiency, lower investment and operating costs, but also due to the higher absorption by metallic surfaces [17, 18]. The later

is the main driving force for the increase in popularity of the HPDL. Due to the dependence of the absorption rate on the wavelength of the incident radiation on the metallic surface, the relative low wavelength of the HPDL promotes an increase in the absorption rate. Consequently, better overall efficiency rates are achieved [15, 16, 18, 19].

2.2. Laser Surface Hardening

Laser surface hardening, a novelty heat treatment, is applied to discrete surface regions of components to improving wear resistance without affecting the microstructural conditions of the bulk material, usually characterized by relatively high toughness levels [3, 7]. It is used to explore the mechanical properties, mainly of steels, by creating complex and unique microstructure combinations. Microstructural changes are responsible for altering properties such as hardness, wear resistance, strength, torsional, and bending fatigue resistance [20, 21]. In its essence, laser surface hardening principles are based on the same principles of conventional hardening, where the main goal is to increase hardness and strength by the transformation of austenite into martensite, designated as quenching. The two heat treatment approaches differ on the size of the region involved. For laser surface hardening, only a thin superficial layer of material is subjected to quenching, leaving the underlying bulk material practically unaffected by the energy supplied. More so, for laser surface hardening, the maximum hardened depth expected is around 2.5 mm [2, 17].

The entire process of laser surface hardening is operationalized around the idea of exposing the component's surface to a thermal cycle of rapid heating and cooling (10^8 to 10^{10} ºC/s), which in the case of steels, enables the austenitization and subsequently martensite transformation [3, 17]. To successfully conduct a surface hardening operation (as illustrated in figure 1), the entire process starts with the projection of the laser beam onto the metallic surface, where only part of the radiation emitted is absorbed. The usual shape of the laser beam for hardening operations is a square or a rectangular shape, and the power density required to accomplish favorable results is between 1000 and 2000 W/cm^2. Still, in some special occasions, it can go as high as 5000 W/cm^2. Such power densities support the

increase of the surface layer's temperature in a relatively short time, ultimately leading to microstructure austenitisation. The underlying bulk material acts as an efficient heat sink causing rapid cooling when the laser beam is no longer acting on a point that was already subjected to the beam radiation. This effect is only possible due to the continuous movement of the laser beam over the workpiece, and it is the result of the self-quenching ability of the materials treated, especially steels. More so, it is due to the self-quenching effect that in laser surface hardening, traditional quenching media (e.g. water, oil, salt bath) aren't needed [1, 2, 7].

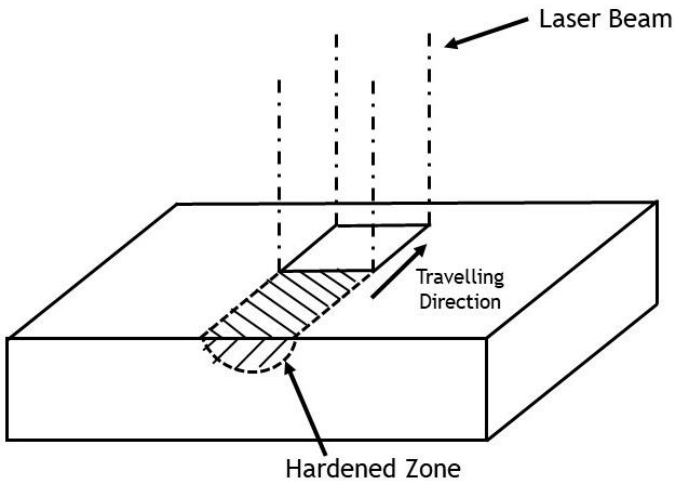

Figure 1- Working principle of Laser Surface Hardening - Adapted from [7]

As previously mentioned, the main goal of such heat treatment is to achieve hardened and possibly highly wear resistance surfaces. Such a phenomenon results from a three-step process, starting with an austenitization step, where the previous microstructure is forced to begin its transformation into austenite, followed by the second step of austenite homogenization and finally, the martensitic transformation via rapid cooling [4].

In the first step, the material is heated to temperatures above the austenitization temperature (A_{c1}[1]), but always bellow the melting temperature [4, 22]. Many factors that determine the ideal austenitization temperature, such as the grade of the steel being treated, or even the microstructural state of the component (grain size and presence of undissolved carbides). Furthermore, due to the intensive

[1] A_{c1}- temperature at which austenite begins to transform during heating [8]

heating rates of the laser hardening process, the entire system is far from the equilibrium conditions. Such unusual conditions promote the movement of the A_{c3} [2] line to higher temperatures, resulting in significantly higher austenitization temperatures than those used during conventional hardening. There is also a restricted time available to perform the heating stage of the heat treatment (around a few seconds), contributing to the increase in the austenitization temperature [1, 7, 17]. In the end, laser hardening parameters are conceived around the idea of heating the steel to a high enough temperature that supports austenitisation, but always limited by the constraints of grain growth and surface melting, both undesirable [7].

In the second step, austenite homogenization is needed to promote the complete austenitization of the microstructure. As laser surface hardening can achieve such extreme heating rates, the microstructural phases need time to transform and homogenize. The extend of this second step is strongly dependent not only on the grade of steel being hardened but also on the previous microstructural condition, in what regards grain size, carbide size and distribution and even on the raised temperature [3, 22]. It is essential to mention that the significant reduction of time given to the austenite homogenization, when compared to the traditional hardening methods, allows time savings but also consents the acquisition, in average, of a grain size far below of what is expected [23].

The third and last step, martensite transformation by self-quenching, is based on a diffusionless and athermal transformation, where martensite forms without any interchange in the position of neighboring atoms, but only involving co-operative movements of atoms over distances less than an atomic diameter [24, 25]. Martensite presents a tetragonal body-centered crystal microstructure (figure 2 (a)). It results from the shear type solid state phase transformation of the austenite with carbon content above a critical value, known as Cc, which is usually taken to be 0.05 wt% C [22, 26]. It is essential to mention that the martensite hardness' is strongly dependent on the extent of the tetragonal distortion, which is evaluated based on the ratio between the c-axis and the a-axis. Knowing that carbon atoms prefer to occupy the interstitial sites along the c-axis (as illustrated on figure 2 (a)), the higher the carbon content, the higher the c/a ratio (also known as tetragonality)

[2] A_{c3}- temperature at which transformation of ferrite to austenite is complete during heating [8]

(figure 2 (b)), which results in a higher hardness value. So it is possible to affirm that the increase in carbon content results in martensite with higher hardness [22].

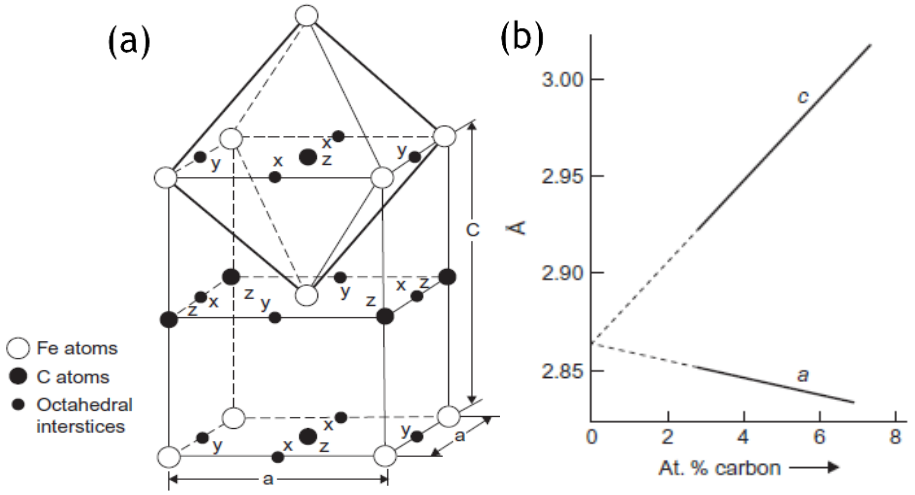

Figure 2- (a) Body-centered tetragonal unit of martensite – Source: [26]; (b) Variation of c and a parameters with carbon content in martensite (where Å is the lattice dimension) – Source:[25]

In the end, after the hardening process through laser technology, it is expected to obtain a microstructural distribution that is divided into three different zones, as showed in figure 3. The first one, at the surface, is the hardened zone (HZ) and it is characterized by having an utterly martensitic structure, and consequently, the highest value of hardness. The transition zone (TZ) consists of a partly austenitised and eventually hardened microstructure, event that strongly depends upon the material being treated but also on the selected parameters. Finally, the base material (BM) presents the initial microstructure of the component before it was subjected to the hardening process [2, 27].

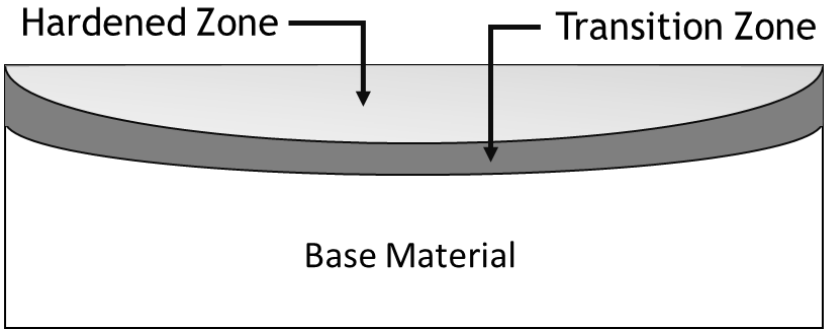

Figure 3- Microstructural zones of Laser Surface Hardening – Adapted from [27]

2.2.1. Process Parameters

One of the main characteristics of laser technology is its ability to adapt with relative ease to different industrial scenarios. To do so, the entire system is endowed with multiple parameters, responsible for the variation of the properties of the produced laser beam, giving the complete system unparalleled levels of flexibility [1]. In particular, for laser surface hardening, the main independently controlled process parameters are (1) power output; (2) spot size and shape; (3) feed rate [3, 16, 28, 29].

The power output is a parameter that affects both the maximum temperature reached at the surface and the heating rate, and it strongly depends upon the power limits of the system in use. The maximum temperature reached during laser surface hardening is also limited by the melting of the surface [7, 29]. Knowing that, for laser surface hardening, the main characteristic to be controlled is the temperature reached during the process, engineers at Fraunhofer IWS developed a system capable of controlling the temperature at the surface by automatically adjusting the beam power. The laser surface hardening process is conducted in conjunction with a camera-based temperature measuring system ("E-MAqS") and a laser power control system ("LompocPro"). By resorting to this system, instead of setting a fixed beam power for laser surface hardening, which leads to temperature fluctuations at the surface during the process, the desired surface temperature for laser surface hardening is set. The beam power is dynamically adjusted according to the inputs from the "E-MAqS" to the "LompocPro" system. The later gives an output to the laser system, adjusting the beam power. Ultimately, by resorting to such advance control systems, the overall energy input promoted by the laser action onto the metallic surface tends to be standardized throughout the entire laser hardening operation. In the end, more homogeneous hardened layers in terms of surface hardness but also hardening depth are expected [2, 30, 31].

Regarding the beam spot size and shape, for laser surface hardening, a laser with a uniform energy distribution is ideal, to provide uniform temperature distribution at the surface [4, 16]. To shape the laser beam to the desired form, there are several methods capable of modifying the beam, known as beam-shaping techniques (beam defocusing, optical integration, beam scanning, and kaleidoscope) [3]. These complex shapes obtained by such methods originate from primitive beam

modes, known as transverse electromagnetic mode (TEM). For laser surface hardening, the more commonly used modes are the TEM_{00} (Gaussian Beam) and the TEM_{01}, which unlike the Gaussian beam, is characterized by having a high level of energy concentrated at the periphery [4]. In general, there are three types of shapes commonly used for laser surface hardening, these being, circular/elliptical pattern and rectangular pattern, originating from the Gaussian beam and the rectangular beam, product of the TEM_{01} beam mode [3]. Depending on the beam shape and size chosen, the width and penetration of the heat affected zones will change due to changes in the power density in what regards its intensity and distribution [1, 3, 32]. Engineers at Fraunhofer IWS developed a dynamic beam shaping system, denominated "LASSY", which is integrated with the previously presented "E-MAqS". Such technology allows a flexible and controlled beam shaping process, unlike the more traditional systems which use a set of optics with fixed spot geometries. In the end, it is possible to adjust the power density distribution and spot size with relative ease [30].

Lastly, the feed rate represents the velocity of the movement of the laser spot relative to the material surface [7]. Typical values of feed rates for laser surface hardening, can range from 5 to 400 mm/s [3]. Such broad-spectrum derivates from the fact that different materials present different dwell austenitization times, due to their metallurgical characteristics, such as heat conductivity and microstructural state. The dwell time will increase with the decrease of the feed rate for the same spot size. More so, the dwell time is directly related to the interaction time; the later is determined not only by the feed rate but also by the spot size [7, 33]. Finally, it is necessary to consider that the broad spectrum of feed rates is also related to different laser types with diverse power outputs.

2.3. High-Speed Steels

High-speed Steels (HSS) belong to the larger family of tool steels, possibly being one of the most elaborate classes of the group as they are capable of combining characteristics from the hot work tool steels, with excellent tempering resistance and hot resistance, but also from the cold work tool steels, capable of meeting requirements for wear resistance and hardness. This complex arrangement of

properties results from an intricate combination of chemical compositions, phase transformation and microstructure [5, 34-36]. High-speed steels own their name to the ability to machine components made from steel and other materials, at extremely high cutting speeds. These high machining speeds result in an increase in the temperature of the tool, meaning that high-speed steels need to present not only high hardness at room temperature but also at high temperatures, also known as red hardness [37]. HSS are high alloy steels, composed by combinations of different alloying elements such as molybdenum (Mo), vanadium (V), tungsten (W), cobalt (Co), and chromium (Cr) in addition to iron (Fe) and carbon (C). The carbon and alloy contents are balanced to enable high hardening response, high resistance to the softening phenomenon and excellent levels of toughness. The solid solution alloying promoted by these elements on the martensitic matrix corresponds to an increase in the hot hardness. Meanwhile, the presence of hard carbides of Mo, W, V and Cr is responsible for the high level of hardness and wear resistance [38, 39]. It is important to understand that all HSS are subjected to a complex sequence of heat treatments that promote the acquisition of a microstructure compose by a tempered martensitic matrix, generally composed by iron and alloying elements, and by undissolved particles. These undissolved particles are carbides uniformly distributed and represent 5 to 20% of the microstructure. [5, 34, 38].

High-speed steels are classified, according to the SAE classification system, as T-series or M-series where the T-series corresponds to the grades where tungsten is the major alloying element (between 12 and 20%), and the M-series are the grades where molybdenum is the major alloying element (between 3.5 and 10%) [37, 38]. From a performance point of view, there is no significant difference between the T and M-series high-speed steels, except that the M-series generally presents higher abrasion resistance and lower distortion levels during the heat treatment procedure. The biggest difference between the two series is the significantly lower cost of the M-series, due to greater availability and consequently lower cost of Mo when compared to W. More so, the cost difference is reinforced by the fact that the atomic weight of Mo is about half of the tungsten. Therefore, less Mo is needed to produce the same results that are achieved when tungsten is the major alloying element, has both elements present similar atomic radius and similar carbide formation. It is essential to mention that the M-series presents a lower melting point, resulting in

lower hardening temperatures and shorter hardening range. Consequently, the red hardness of the M-series HSS is negatively affected, effect that can be easily overcome by the addition of residual content of tungsten and to some extent vanadium (SAE M2, M3 and M4 grades). For all the reasons above presented, nowadays, the M-series high-speed steels represent about 85% of all tool steels [5, 38, 39].

All HSS grades have similar mechanical and physical properties, where slight property changes are possible due to the distinct chemical composition of each single grade. The most important property for all HSSs is the cutting ability, which can be evaluated taking into account four characteristics: (1) hardness ; (2) hot hardness; (3) wear resistance; (4) toughness [37]. More so, all HSSs, no matter the grade and/or chemical composition, present sufficient carbon content to achieve hardness values of 64 HRC, high depths of hardening, and for small cross-sections, it is possible to harden in still air [39].

2.3.1. SAE M2 High-Speed Steel

In today's tool making industries, the SAE M2 is perhaps the most important HSS in existence, with a good balance between tungsten and molybdenum. It is due to its chemical composition, in combination with mechanical properties, that the SAE M2 is capable of responding to different mechanical requests with an excellent performance [5, 40, 41]. The popularity of the SAE M2 steel dates back to the 1950s, when due to the shortage of metallic raw material during World War II, manufactures were forced to look for alternatives, mainly replacing tungsten and vanadium with molybdenum [39, 42]. The SAE M2 can be employed in both cold and hot work tools. Nonetheless, the most common application for this grade of HSS is its use as cutting tool material, being one of the reference HSSs in this particular area. Some particular applications are general-purpose drills, end mills, reamers, milling cutters, among others [5, 37].

Regarding its chemical composition, and according to the ASTM A600 − 92a:2016 standard [43], the minimum and maximum requirements for each chemical element are presented in table 1. The SAE M2 is characterized by having a controlled and high content of Mo and other alloying elements and is further

classified according to the carbon content. The later could be defined as a SAE M2 with regular carbon content or high carbon content.

Table 1- Chemical composition requirements for the SAE M2 steel - Adapted from [43]

	C		Mn		P	S	Si		Cr		V		W		Mo	
	min	max	min	max	max	max	min	max	min	max	min	max	min	max	min	max
Regular C	0.78	0.88	0.15	0.40	0.03	0.03	0.20	0.45	3.75	4.50	1.75	2.20	5.50	6.75	4.50	5.50
High C	0.95	1.05	0.15	0.4	0.03	0.03	0.20	0.45	3.75	4.50	1.75	2.20	5.50	6.75	4.50	5.50

Values presented in percentage (%)

2.3.1.1. Carbides

As mention before, the unique mechanical properties of the HSSs regarding their hardness at room and high temperatures and wear resistance is a result of the complex combination of the effect of the alloying elements on the steel matrix as well the formation of highly complex carbides during solidification, usually resulting in a microstructure composed by martensite strengthened by alloying carbides [5, 44]. As shown in figure 4, image representative of a SAE M2 microstructure after tempering, the microstructure is composed by a tempered martensitic matrix with a large amount of carbides randomly disperse (white “spherical” particles) [41].

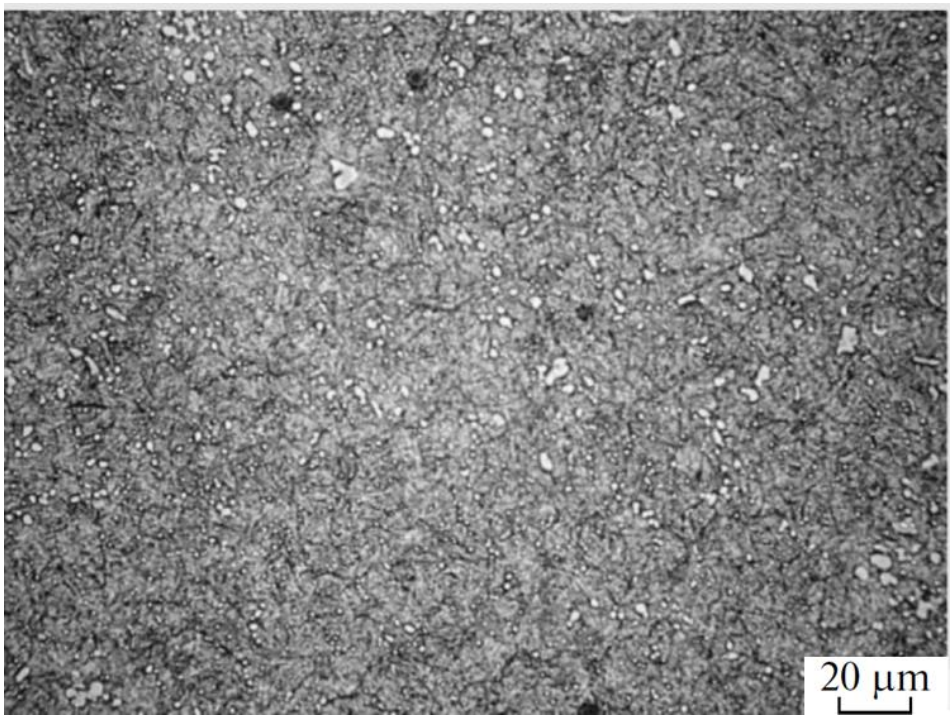

Figure 4- Microstructure of a conventional tempered SAE M2 – Source: Chaus [41]

There are a vast number of possibilities in what regards the typology of carbides present in an HSS, as these are strongly dependent on the steel composition but also the heat treatment history. According to the literature [5, 36, 40-42, 45], the most common carbides in a SAE M2 after tempering, are the MC and M_6C types, with sometimes small traces of the $M_{23}C_6$ type. The MC carbide is a vanadium-rich carbide; the M_6C corresponds to a carbide rich in molybdenum and iron; and the $M_{23}C_6$ a chromium-rich carbide [46]. Both the MC and M_6C carbides have a face-centered cubic (FCC) structure, despite having distinct chemical compositions. For the M_6C, observed in almost all HSS, M stands for Fe, but also to W, Mo, V, and Cr [39, 42]. Meanwhile, the MC type carbide is formed by the amount of V above the solubility limit, which for a HSS with carbon content of approximately of 1% is about 1% of V [5, 45]. Apart from this, the two primary carbides also differ on the hardness, where the MC carbide presents a value between 2800 and 3000 HV and the M_6C carbide presents a value of approximately 1500 HV [45].

Another significant phenomenon regarding carbides in the SAE M2, is the fact that despite after heat treatment, the carbide structure being composed by mainly MC and M_6C carbides, the as-cast carbide structure presents one more carbide type, the M_2C, a molybdenum-rich carbide. The as-cast eutectic carbides formed during

solidification are the MC, the M_2C, and the M_6C carbides (also known as eutectic carbides) [5, 42, 44, 47]. After solidification, the as-cast SAE M2 products are subjected to annealing and hot working (for example, hot rolling or forging). In this process, the as-cast microstructure is broken down, and due to the low thermostability of the M_2C, the metastable carbides transform according to equation 1, improving the microstructural homogeneity of the steel by disrupting the former coarse as-cast networks of carbides [5, 34, 41, 44].

$$\mathbf{Eq.1} \quad M_2C + \gamma\,(Fe) \rightarrow MC + M_6C \qquad [44]$$

According to Chaus [41], who conducted a study on the structural and phase transformations during heat treatment of a SAE M2, it became clear that at temperatures above 1200 ºC, the steel begins to precipitate particles during the decomposition of the M_2C carbide. In a similar study conducted by Liu *et al*. [36], and resorting to the experimental differential scanning calorimetry (DSC) curve during heating of a SAE M2 at a rate of 200 ºC/h, it was possible to determine the temperatures of the decomposition reactions. From 897.2 to 1221.5 ºC, the M_2C carbide decomposes. Bellow 1120 ºC, the decomposition is relatively slow, but above this temperature, the kinetics of the reaction increase significantly. Above 1221.5 ºC, the newly formed carbides M_6C and MC begin to dissolve into the liquid, until 1420 ºC where the solid is completely transformed into liquid.

The decomposition and nucleation of the different carbides change according to their nature and chemical composition. According to Zhou *et al*. [44], the M_6C carbide forms at the M_2C/matrix interface, region at which they obtain the required elements from the M_2C and the steel matrix. This process enriches the regions around the M_6C carbide with vanadium, considering their chemical composition (Table 2), vanadium isn´t in a large amount. This enrichment process makes the regions around M_6C carbides excellent nucleation zones for the MC carbide, as they are a vanadium-rich carbide. Due to their nucleation nature, the M_6C and MC carbides present a different behavior regarding the variation in the holding time at high temperatures. For the same high temperature, the increase in the holding time promotes the content increase of the M_6C but the decrease of the content of the MC carbide, despite both being a product of the decomposition of the M_2C carbide that

increases with the increase in the holding time. This particular phenomenon is the result of the chemical composition of each carbide, where during the decomposition of the M_2C carbides, a significant amount of Fe atoms diffuse to participate in the formation of the M_6C carbide, meanwhile the MC carbide results from the vanadium content gradients.

Table 2- Chemical composition of the M_2C carbide and the decomposition products, the MC and M_6C carbides – Adapted from [48]

	W	Mo	V	Cr	Fe
M_2C	42.0 ± 6.6	28.9 ± 5.9	**13.6 ± 1.3**	6.8 ± 0.9	5.1 ± 2.6
MC	19.9 ± 6.7	12.7 ± 3.3	**49.2 ± 5.2**	4.2 ± 2.0	3.1 ± 1.8
M_6C	33.9 ± 3.9	23.8 ± 2.6	**3.8 ± 0.9**	4.3 ± 0.7	32.5 ± 1.3

Values presented in mass percentage (%)

2.3.1.2. Conventional Heat Treatment

The heat treatment stage for any HSSs is one of the key elements for its properties. It is only by executing the correct heat treatment sequence that is possible to obtain the expected hardness and wear resistance. Every single grade of HSS presents specific temperatures and holding stages, but for the most part, it comprehends a preheat cycle, quenching and tempering treatment (with relatively short holding stages). All HSSs present a strong secondary hardening effect on tempering, due to the precipitation of large quantities of carbides from the supersaturated martensite, previously formed on quenching [5, 34, 49]. The appropriate temperatures for each heat treatment stage for the SAE M2 are presented in table 3, values stipulated by the A600-92a:2016 standard [43]. Such temperatures are only a general recommendation for the ideal conditions. Consequently, other combinations of austenitizing and tempering temperatures can be used depending on the intended application. By resorting to the study conducted by Adaskin [40], in which are explained the temperature combinations according to the possible application of the SAE M2, it is clear that depending on the purpose, the heat treatment conditions will differ. For cutting tools, the principle of sufficient

strength dictates the entire heat treatment. So, the maximum possible quenching temperature is selected to promote strong M_6C carbide precipitation but constrained by the need of sufficient strength to prevent fracture or chipping of the cutting edge. With this kind of temperature selection, it is possible to ensure maximum hardness and maximum tool life. Another approach possible is the principle of sufficient hardness. For example, in the case of dies production, it is essential to ensure a relative high compressive yield point to resist crumpling, and at the same time, thermal stability, since in the case of stamping dies, operating temperatures can rise up to 400 ºC. In this case, when heat treating, the quenching temperature must be set to a level that enables slight carbide precipitation, ensuring sufficient hardness and compressive yield point, thus maximum tool life [40].

Table 3- Temperature heat treatment requirements for the SAE M2 – Adapted from [43]

	Preheat (°C)		**Austenitizing (°C)**		**Tempering (°C)**	**Hardness (HRC)**
	min	max	Salt Bath	Controlled Atmosphere Furnace		min
Regular C	732	843	1216	1227	552	64
High C			1204	1216		65

Figure 5 represents the diagram of the conventional heat treatment cycle for the SAE M2. The heat treatment cycle is divided into three different stages: A- preheat stage, B- quenching stage, and C- tempering stage. The aim of the preheat stage is to reduce thermal shock, minimizing the possibility of high levels of distortion and cracking. Still, it is also capable of reliving possible stresses caused by previous machining steps. The preheat stage is also responsible for minimizing possible carburization or decarburization if the atmosphere in the furnace is not inert. It can be taken as a step where the steel molecules are preconditioned for the next transformation, the austenitization of the microstructure [37, 49]. There are several approaches regarding the temperature and time for the preheat cycle, but for the most part, the preheat cycle is divided into two different holding levels. The first one, at 650 ºC, for 10 to 15 minutes, and the second one at 845 ºC, for 10 to

15 minutes. It is crucial to understand that the holding time is strongly dependent on the size and thickness of each part being heat treated, so the holding time must be adjusted according to the cross-section of each part [49].

The second stage, quenching, comprehends the austenitization of the microstructure, followed immediately by the rapid cooling, enabling martensite transformation. For HSSs, particularly for the SAE M2, the austenitization is responsible not only for the transformation of the previous metallurgical phases, most commonly ferrite to austenite, but also for the dissolution of the complex carbides. The extent of this dissolution will strongly affect the following heat treatment stages, and most of all, the properties of the high-speed steel. The temperatures required for the effective dissolution of the carbides is very close to the solidus temperature. For quenching SAE M2 steel: austenitization temperature should be between 1175 and 1245 ºC and dwell times should range from 1 to 5 minutes, depending on the size of the parts. The relative short dwell times are used to avoid grain growth. More so, the use of a lower level of temperatures are associated with heat treatments for parts that require high levels of impact toughness, and the higher levels of temperatures are associated with high levels of hardness and red hardness [5, 37, 49]. After the appropriate austenitization of the microstructure, a rapid cooling cycle must be conducted. All HSSs present excellent hardenability and are deep hardened. The quenching media strongly depends upon the size of the cross-section of every single part and the grade of HSS being heat treated. For some grades, a two-step quenching process is needed, initially in a molten slat bath or oil, and then by air cooling. For relative thin cross-sections, the quenching process can be done by air cooling [37].

The third and last stage, tempering, is executed to promote the secondary hardening effect, a distinctive characteristic of all HSS grades, as well as to transform possible retained austenite and even stress reliving [37, 50]. The tempering stage can comprehend a double or triple treatment, a fact that not only depends on the extent of the retained austenite transformation, but also on the shape of the part being treated and the hardness needed for a certain application. Every single cycle is conducted bellow the critical transformation temperature (A_{c1}), with holding times of 2 hours per 25 mm, followed by cooling. The temperatures will vary according to the expected final hardness and HSS grade. Each single grade

presents an ideal temperature for maximum hardness or minimum hardness, and consequently, maximum toughness [37, 49]. According to Bryson [49], for the SAE M2, the first tempering cycle should be conducted at 565 ºC followed by a second at 550 ºC and a third (the last one) at 540 ºC. More so, the author advices that the first tempering cycle must be done immediately after the quenching stage at a temperature between 52 and 65 ºC. The constant reduction of temperature between stages is responsible for maintaining the original tempering hardness level.

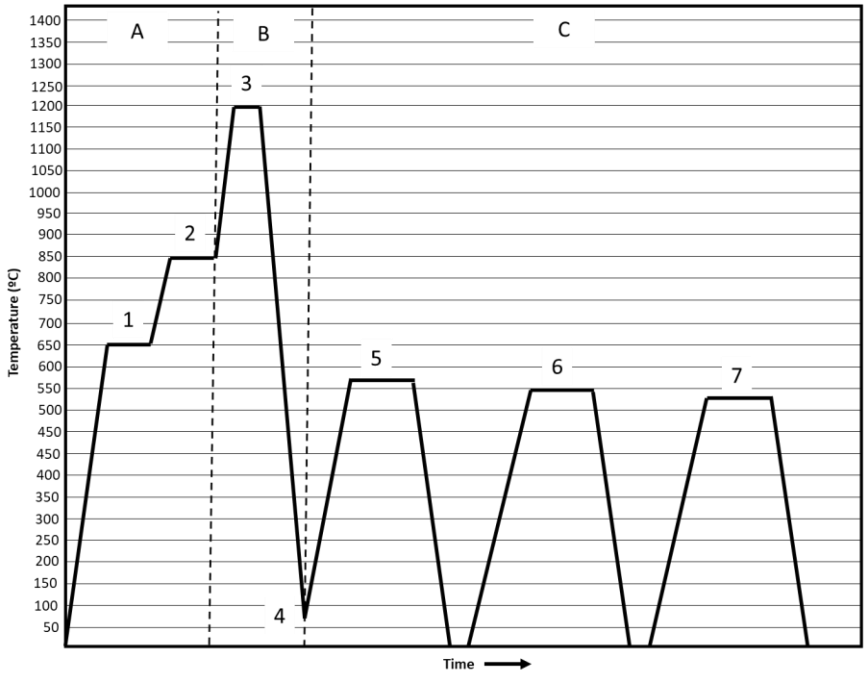

A	Preheat
B	Quenching
C	Tempering
1	650 ºC for 10 to 15 min.
2	845 ºC for 10 to 15 min.
3	1175 to 1245 ºC for 1 to 5 min.
4	52 to 65 ºC
5	565 ºC for 2 h/25 mm
6	550 ºC for 2 h/25 mm
7	540 ºC for 2 h/25 mm

Figure 5- Conventional heat treatment diagram for the SAE M2 – Adapted from [49]

3. Experimental Procedure

Considering the goals of the dissertation, the experimental work comprehended two separate heat treatment processes. Laser surface hardening was first studied, followed by a tempering heat treatment analysis on the previous laser hardened material with the established optimal process parameters, as shown in figure 6. In both cases, annealed base and conventional hardened and tempered base material was heat treated.

Both heat treatment studies followed an analogous experimental procedure. First, heat treatment conditions were defined. More specifically, for the laser surface hardening process, the definition of the process parameters and for the tempering heat treatment, the definition of the tempering temperatures. After conducting the tests, extensive mechanical and microstructural characterization was performed via surface hardness and hardening depth analysis, but also, by resorting to optical microscopy (OM), X-ray diffraction (XRD) and scanning electron microscopy/energy-dispersive X-ray spectroscopy (SEM/EDS) analysis.

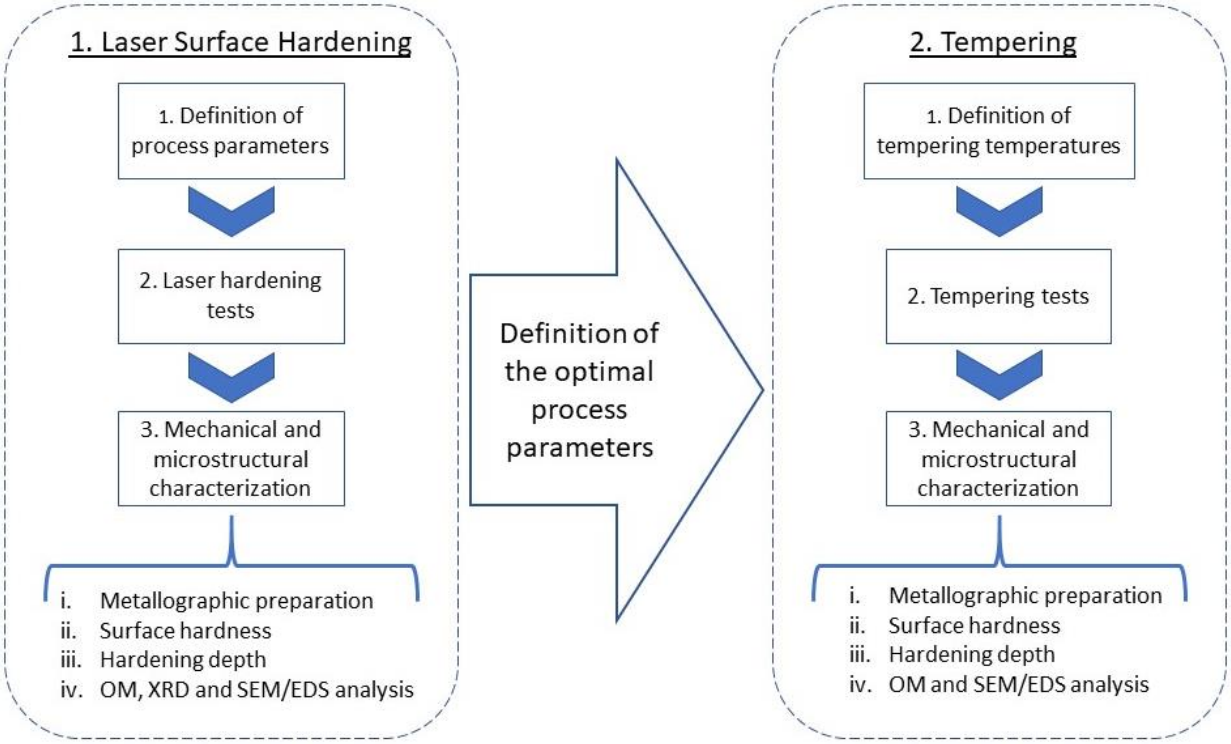

Figure 6- Schematic representation of the experimental procedure

3.1. Materials

The material used in this study was a SAE M2 in two different metallurgical states: annealed state (A) and conventional hardened and tempered state (B). The chemical composition of the received material is presented in table 4. By comparing such chemical composition to the previously shown chemical compositions for the SAE M2 by the ASTM A600-92a:2016 standard [43], the particular grade of high-speed steel in the study, belongs to the family of SAE M2 with relatively high carbon content.

Table 4- Chemical composition of the tested SAE M2

C	Si	Mn	P	S	Cr	Mo	W	V
0.94	0.45	0.4	0.03	0.03	4.5	5.2	6.7	2.1

Values presented in percentage (%)

According to the supplier's datasheet, the conventional hardened and tempered SAE M2 was subjected to a last tempering stage at 530 ºC resulting in a hardness of 60 ± 2 HRC. No further information regarding the temperatures of the conducted heat treatments on the as-received SAE M2 in both metallurgical states was supplied.

Furthermore, microstructural analysis and hardness evaluation were conducted, according to the procedure presented in subchapter 3.4. Mechanical and Microstructural Characterization on both delivered state materials. These results are important to create a baseline for comparison when evaluating the laser surface hardening responses.

3.2. Laser Surface Hardening Process Parameters

By resorting to Fraunhofer's IWS equipment and methodologies for laser surface hardening applications, and considering all the internally developed systems for laser process monitoring and control, the process parameters to be defined during experimental work were the (1) surface temperature, (2) spot size and shape and (3)

interaction time. Furthermore, when defining the process parameters, the previous laser hardening and melting studies [6, 8, 9, 51-57] were considered, as a starting point to the different parameters (Appendix I). The laser system used for this research work was a high-power diode laser (HPDL), Laserline LDF5000-400 integrated with Laserline zoom optics.

The first step for the experimental work was defining the maximum operating temperature possible without surface melting. To do so, several laser passes were conducted starting at a temperature around 1250 ºC and progressively increasing the temperature in steps of 20 ºC. The increase of the temperature was suspended when, via microscopic analysis, traces of surface melting were identified. After established the occurrence of surface melting, the temperature was decreased in steps of 10 ºC, until microscopic analysis showed no evidence of surface melting. At this point, the maximum operating temperature for laser surface hardening was set to 1290 ºC. By resorting to such methodology, it is possible to laser surface hardening at temperatures 10 to 20 ºC below the melting temperature, thus maximizing the hardening effect [58].

In what regards the spot size and shape and taking into consideration that most of the operations conducted at Fraunhofer IWS are addressed to industrial applications, the smallest size in use, for this particular field of operations, is a square laser spot with 10 mm in length by 10 mm in width.

The following step, regarding the experiment work, was the execution of various surface hardening operations, adjusting the interaction time. The interaction times set for the experiment work were defined based on previous works conducted at Fraunhofer's IWS facilities in conjunction with the staff's experience. As listed in tables 5 and 6, the interaction time displays an increase according to the geometric sequence, $a_n = 0.5 \times 2^{n-1}$, starting at 0.5 s until 16 s. Such mathematical evolution provides a good balance between a viable number of experiments, in industrial environment, and a high level of accuracy regarding the optimal process parameters. More so, in table 6, the feed rates for each individual experiment are presented. The sample dimensions for the laser surface hardening operation were set to 20 mm in width by 10 mm in height by 100 mm in length.

Table 5– Defined process parameters for the laser surface hardening experiments

Temperature (ºC)	1290
Spot Size (mm)	Square Shape 10 x 10
Interaction Time (s)	0.5 1 2 4 8 16

Table 6– Resulting feed rates for the defined process parameters

Dimension of the laser spot on the traveling direction (mm)	**Interaction Time (s)**	**Feed Rate (mm/s)**
10	0.5	20
	1	10
	2	5
	4	2.5
	8	1.25
	16	0.625

In the end, after laser surface hardening, twelve samples were produced, six samples originated from the annealed SAE M2 (A family samples), and six other samples, from the conventional hardened and tempered SAE M2 (B family samples). The analysis of the samples, to determine the optimal process window, took into consideration two characteristics, surface hardness, and hardening depth. To do so, macro and low-force hardness tests were carried out, as well as microstructural analysis, following a set of rules of sample selection and execution, which are described in detail on subchapter 3.4. Mechanical and Microstructural Characterization.

Each individual sample was correctly identified, following an alphanumeric system, maintaining the traceability throughout the different experiments conducted. Figure 7 displays an example of the code system used to categorize the samples. The first letter of such a code system concerns the base material state. The letter A corresponds to the annealed state and the letter B to the conventional hardened and tempered state. The following number corresponds to interaction time during laser heat treatment used, starting with 0 to the non-laser heat-treated samples, all the way up to 6, corresponding to an interaction time of 16 s.

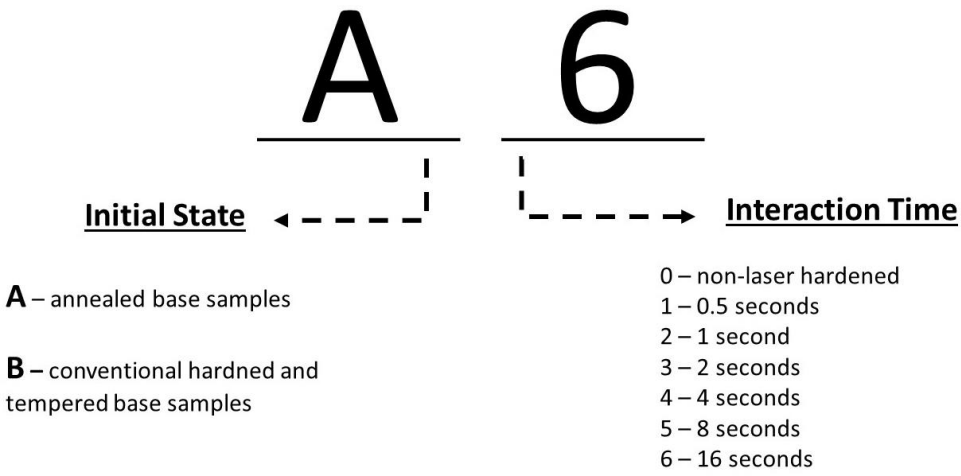

Figure 7– Code system used for the samples' identification

3.3. Tempering Evaluation

The tempering heat treatment study started with the definition of the tempering temperatures to which, the laser surface hardened SAE M2 was subjected. The selected tempering temperatures were 350, 450, 475, 500 and 550 ºC with holding times of 2 hours, following the previous mention rule of 2 hours per 25 mm. Only the laser surface hardened samples, processed with the previously established optimal parameters, were subjected to a posterior set of tempering heat treatments. One safety measurement taken was the use of a "protective bed" composed by charcoal and steel chips whenever the samples were loaded onto the furnace, significantly minimizing the decarburization of the test samples during the tempering heat treatment.

The tempering curves were based on the evaluation of the surface hardness, latter supported by hardening depth determination and microstructural evaluation, for the temperatures that presented maximum secondary hardening effect. As a term for comparison, a tempering curve for the conventional heat-treated SAE M2 was also developed, with the above mention tempering temperatures. To do so, before the tempering evaluation, the as-received annealed samples were subjected to a previous hardening stage at 1210 ºC, in a controlled atmosphere furnace, using argon, for 15 minutes and quenched in atmospheric air.

3.4. Mechanical and Microstructural Characterization

The characterization segment of the previously conducted experimental work was carried sequentially, following a logical progression as described in this subchapter. Such a pragmatic approach maximizes efficiency in what regards time and lab work. The first property analyzed in all the samples produced was the surface hardness. Secondly, hardening depth analysis was conducted, followed by optical microscopy, XRD, and SEM/EDS analysis, methodologies in which extensive metallographic preparation was necessary.

3.4.1. Surface Hardness

The measurement of the surface hardness for all the specimens was carried out by resorting to the Rockwell C hardness test, according to the standard ISO 6508-1:2016, except for the annealed SAE M2 (specimen A0), which was evaluated by resorting to Brinell hardness test, according to the standard ISO 6506-1:2014. The hardness evaluation of the as-received annealed and conventional hardened and tempered specimens, did not follow any particular rule regarding selecting the indentation site, only assuring that the specimens' surface was geometrically flat and clean. The laser hardened specimens followed a stricter rule for selecting the indentation site, by conducting them only on the center of the laser track. More so, for each individual specimen, six indentations were executed to establish a hardness value with reasonable model representativity and standard deviation.

Due to the good surface quality of the specimens analyzed and attending to the surface requirements of the Rockwell C and Brinell hardness tests, there was the need to conduct a slight metallographic preparation by grinding the surface using a 1000 mesh sandpaper with water lubrication instead of the bellow described.

3.4.2. Metallographic Preparation

Before conducting the hardening depth measurements, optical microscopy (OM), XRD and SEM/EDS analysis the specimens were subjected to thorough metallographic preparation. First, all the laser hardened samples were cut

perpendicular to the laser traveling direction, producing cross-sections that provided suitable specimens for the following characterization techniques. More so, an automatic cutting machine, equipped with an abrasive disk, was used to set a low cutting speed, to preserve the specimen's edges. A targeting sampling technique was adopted by carefully eliminating the laser hardened specimens' edges, 10 mm on each side.

To preserve sharp edges all around the specimens' surface during the grinding and polishing steps, the previously cut cross-sections were cold mounted in a two-part epoxy resin, with a hardening time of around 12 hours.

The mounted specimens were first grinded with a coarse silicon-carbide sandpaper, followed by successively finer grits. The complete sequence was composed of 120, 180, 320, and 600 mesh passes. All the grinding stage was executed by resorting to a polishing machine at 300 rpm always with water lubrication. The polishing stage was first performed by resorting to a polishing cloth and 6 µm diamond suspension at a revolution speed of 150 rpm. After a few minutes, both the polishing cloth and diamond suspension were change to a 1 µm diamond suspension and respective polishing cloth, at the same revolution speed.

Only the specimens subjected to OM and hardening depth analysis were etched by immersion technique in an unusual combination of etchants, 2% Nital mixed with 4% Picral. More so and attending to the characteristics of the XRD and SEM/EDS analysis, there was the need to unmount the specimens. After unmounted, the specimens were subjected to another polishing stage before their analysis.

3.4.3. Hardening Depth

For the hardening depth determination, the approach taken was the construction of hardness profiles. Two standards were employed to properly conduct the test, the ISO 18203:2016, regarding the thickness of surface-hardened layers of steels and the ISO 6507-1:201, for the Vickers hardness test. Considering the rules established by both standards, low-force Vickers tests were carried out, with indentation times of 15 s and applied forces of 2.942 N, in 0.1 or 0.2 mm steps between indentations, depending on the prior indention size.

For the laser hardened specimens on the annealed base material, A family, the hardening depth was determined by following the hardness limits provided by

the ISO 18203:2016 standard. For the laser hardened specimens on the conventional hardened and tempered base material, B family, the above mentioned methodology isn't feasible. So, the hardening depth was determined when the hardness value of the indentation is equal to the average of the non-laser treated conventional hardened and tempered hardness.

3.4.4. Optical Microscopy, XRD and SEM/EDS Analysis

To properly characterize all the microconstituents present in the microstructure of the different specimens, optical microscopy is not endowed with enough magnification/resolution to determine with accuracy the exact constitution and morphology of the different microconstituents. For that reason, it was necessary to complement the optical microscopy results, with XRD and SEM/EDS analysis. For the optical microscopy, the LEICA DVM6 digital microscope was used for all microstructural observations, capable of producing images with magnifications up to 2000x. Regarding the XRD analysis, its execution enabled the accurate determination of the carbides present in each individual microstructure. Only the as-received material in the annealed and conventional hardened and tempered state were analyzed as well as the best laser hardened specimens, regarding the maximum hardening depth and surface hardness, for both initial states. The equipment used for the XRD analysis was a Bruker D8 Discover, Bragg-Brentano, with copper Kα radiation ($K\alpha_1$ = 0.15406 nm, $K\alpha_2$ = 0.154439 nm, and $K\alpha_3$ = 0.139222 nm). Finally, the SEM/EDS analysis was conducted by resorting to a FEI Quanta 400 FEG ESEM / EDAX Genesis X4M equipment.

4. Results and Discussion

The results are presented following the experimental procedure chapter, where first analysis of the laser surface hardening process is conducted, followed by the tempering evaluation.

The study of the laser surface hardening process follows a line of thought: firstly, the hardness results are analyzed and discussed, and then microstructural characterization is presented. Such an approach tries to use the surface hardness and the hardening depth results as eliminating factors, in order to select the optimal process parameters. By the end of the hardness analysis, a single interaction time corresponds to the optimal process parameter for each initial microstructural state. After selection, the laser hardened specimens with the optimal process parameters and the base material specimens were subjected to a microstructural analysis.

The tempering evaluation starts with a comparative study of the expected tempering curves, between the conventional and the laser surface hardening heat treatments. Such an approach allows the analysis of the influence of the previous laser processing on the tempering heat treatment. After that, a hardening depth study on the tempered laser surface hardened specimens, at secondary hardening peak, was conducted and their microstructural analysis.

4.1. Hardness Analysis

As the above mention, the hardness analysis is composed of two different hardness tests, surface hardness, and hardening depth. Combining the results for each test allows the selection of the optimal interaction time, where a concept of maximum surface hardness and hardening depth is followed.

4.1.1. Surface Hardness

The first step for the surface hardness analysis was the characterization of the as-received base material, specimens A0 and B0. The specimen A0, correspondent to the as-received annealed SAE M2, presents a hardness of 222 ± 2 HBW 2.5/187.5. Such hardness is in accordance with the bibliographic data [59], were values range

from 212 to 241 HB. Meanwhile, the specimen B0, relative to the conventional hardened and tempered material with no laser processing, presents an experimental hardness of 61 ± 1 HRC. Such hardness is in accordance with the material provider's specifications, previously introduced on subchapter 3.1., and is within the hardness parameters defined by other bibliographic sources [51, 52]. Additionally, as-quenched SAE M2 was produced during the tempering evaluation, which presents hardness values of approximately 66 ± 1 HRC.

Figure 8 displays the evolution of the surface hardness as the interaction time increases, for the laser hardened annealed base specimens (A family). As it is possible to observe, the increase in the interaction time leads to a progressive increase in the surface hardness. Such a phenomenon relates to the fact that longer interaction times result in higher dwell times, which increases carbide dissolution. Consequently, greater levels of martensite transformation will be achieved during cooling, resulting in a more refined and homogenous martensite, ultimately leading to higher hardness values [6, 8].

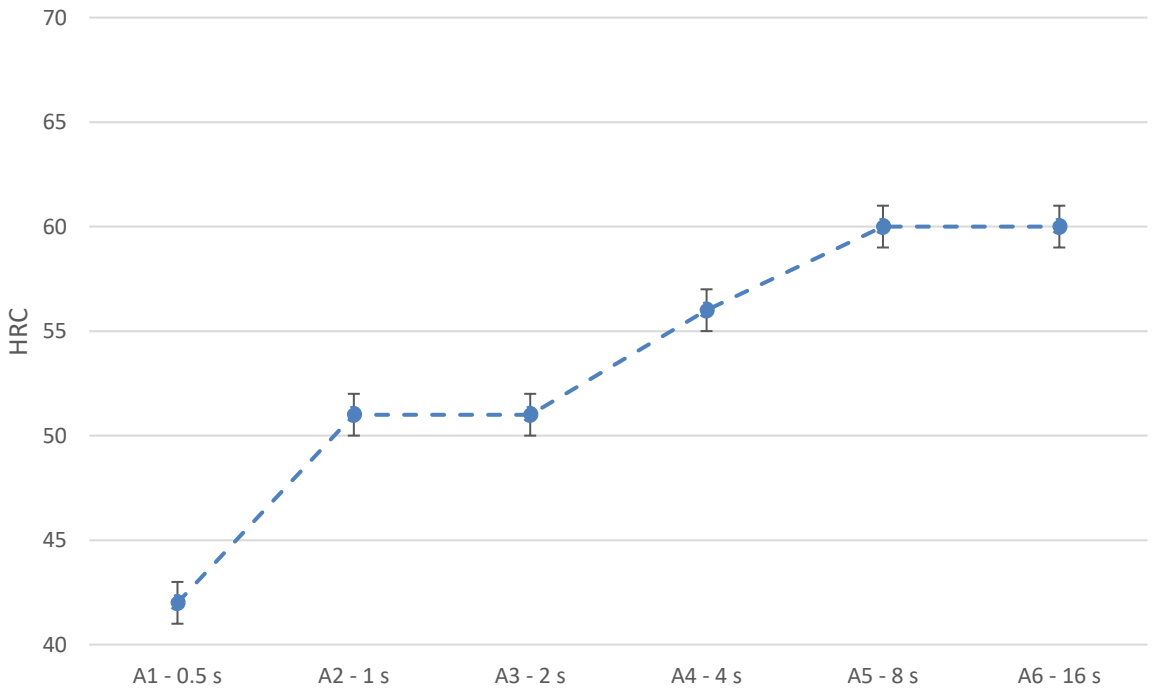

Figure 8- Influence of the interaction time on the surface hardness for laser hardened annealed base specimens

A surface hardness increase of about 43% is observed, from the shortest interaction time (specimen A1 – 0.5 s) to the longest (specimen A6 – 16 s). Such increase not only indicates the presence of large microstructural dispersion between specimens at the surface but also underlines the significant influence of the process parameters on laser hardening. Both the A5 and A6 specimens display surface hardness's (approximately 60 ± 1 HRC) similar to those of the as-received conventional hardened and tempered SAE M2 (61 ± 1 HRC). Even though both groups of specimens aren't in the same microstructural condition, it still is a strong indication that the laser-based heat treatment can achieve similar results to those obtained during the conventional heat treatment.

Despite this fact, when resorting to a laser-based system for surface hardening, its primary is to extrapolate the capabilities of the traditional system by achieving exceptional hardness values. More so, and by analyzing the as-quenched hardness of the specimens produced "in-house" (66 ± 1 HRC) it is evident that there is still room for improvement. In this case, the laser surface hardened specimens present significantly lower surface hardness when compared to the as-quench specimens. It is then possible to conclude that longer interaction times should be explored until reaching an inflection point. Nonetheless, the current surface hardness results demonstrate the capability of such hardening technology on this grade of tool steel.

Regarding the surface hardness of the B family specimens (conventional hardened and tempered base material) after laser hardening, and by observation of figure 9 the surface hardness behavior to an increase in the interaction time is quite different from the previously observed in the A family. In this case, the surface hardness rapidly increases from the base value of 61 ± 1 HRC, specimen B0, to 69 ± 1 HRC, in specimen B1. From this point on, the increase in the interaction time does not promote any variation in the surface hardness. Instead, it remains constant all the way up to an interaction time of 16 s. Therefore, the optimal process parameters will be set only by the interaction time that promoted maximum hardening depth, since all the laser hardened specimens from the B family present equal surface hardness.

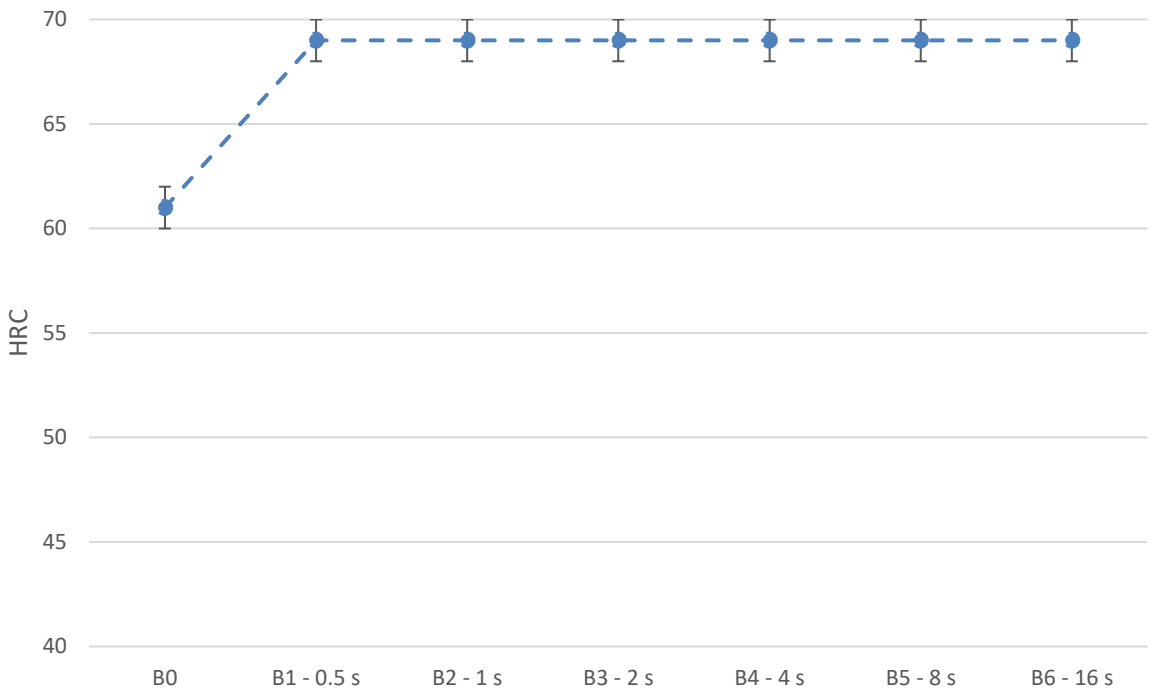

Figure 9- Influence of the interaction time on the surface hardness for laser hardened conventional hardened and tempered base specimens

The only feature that could have led to such distinct behavior, between both initial microstructural states, is the metallurgical condition of the material prior to laser surface hardening. In the case of the B family, potential tempered martensite characterized the base material. Meanwhile, the A family specimens were laser hardened from an annealed base material, where a ferritic microstructure is expected. Both microstructures are presented during the microstructural characterization, subchapter 4.2., in figure 20 and 14, respectively. It can be concluded that the prior heat treatment history of the material strongly affects the surface hardness behavior during laser processing. In other words, the initial microstructural state will pre-define the end results of laser surface hardening operations.

In the high speed steels family, only the so-called super high-speed steels category can achieve hardness values as high as 69 ± 1 HRC, in the tempered state. The addition of Co content in values around 8% followed by an increase in the Mo amount for the M series HSS results in the development of this “super” category of HSSs. The increase in hardness is promoted by the higher precipitation of carbides that the Co addition supports [5]. Considering the as-quenched hardness of the laser

surface hardened B family specimens of approximately 69 HRC, the laser surface hardened SAE M2 could possibly be an alternative to the super HSSs. However, further analysis to understand the surface hardness evolution of the laser surface hardened specimens after tempering. Consequently, the development of the current comparison is completed upon tempering evaluation, subchapter 4.3.

4.1.2. Hardening Depth

After selected the interaction times that allowed maximum surface hardness, the hardening depth analysis will determine which interaction time promotes maximum hardening depth.

Starting with the A family specimens, figure 10 represents the evolution of the hardening depth with the increase of the interaction time. By considering the previous results, relative to the surface hardness, the two most relevant specimens to further analysis are the A5 and A6 specimens, as both present maximum surface hardness. By studying of the hardening depth values available in figure 10 it is possible to conclude that the specimen A6 is the one with optimal response to laser surface hardening. An interaction time of 16 seconds allows the acquisition of a specimen with maximum surface hardness, around 60 ± 1 HRC, and at the same time maximum hardening depth, of approximately 0.8 mm.

By evaluating the hardening depth response to the increase in interaction time, it becomes evident that similar to what is observed for the surface hardness, the hardening depth increases with the rise of the interaction time. This behavior is explained by the larger volume of material that is subjected to sufficiently high temperatures that, upon cooling transforms to martensite. Just like the surface hardness, the increased interaction time leads to an increase in the total energy input during laser hardening, ultimately increasing the hardening depth [6, 9].

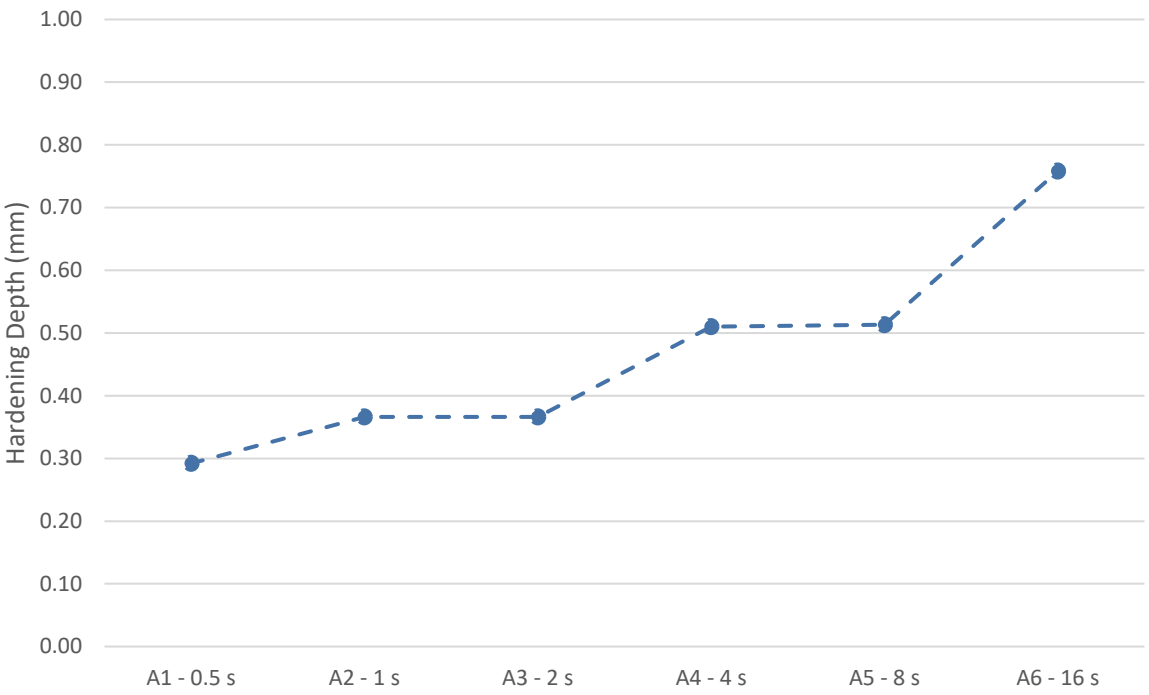

Figure 10- Influence of the interaction time on the hardening depth for laser hardened annealed base specimens-

For the laser hardened specimens with conventional hardened and tempered base material (B family), the hardening depth curve (figure 11) presents a significantly different behavior from the previously discussed. In this case, a maximum inflection point is observed for the specimen laser hardened with an interaction time of 8 seconds (specimen B5). The specimen B5 is characterized by portraying a hardening depth of approximately 1.0 mm and as previously established, a surface hardness of 69 ± 1 HRC. Unlike the A family specimens, in this case, it is possible to state that definitive optimal process parameters were determined as an inflection point was reached, in the form of a pronounced spike. The approach taken during the design of the experiments paid off in the study of the conventional hardened and tempered specimens, as the exponential increase of the interaction time enabled the appearance of such pronounce variation on the hardening depth. If longer interaction times than 8 s are employed during laser surface hardening, a decrease in the hardening depth is observed. This is possibly related to an excessive total energy input during laser hardening, heat soaking the material. Perhaps, such an effect could result in the decrease of the cooling rates in the deeper areas, to rates that don't promote martensite transformation, ultimately leading to hardening

depth decrease. The same hardening depth behavior is observed in the case of employing interaction times lower than 8 s. However, in this case, and as described by W. Liu *et al*. [9], the total energy input is not powerful enough to promote the austenitization of the microstructure in deeper areas of the specimens, consequently not supporting the quenching effect.

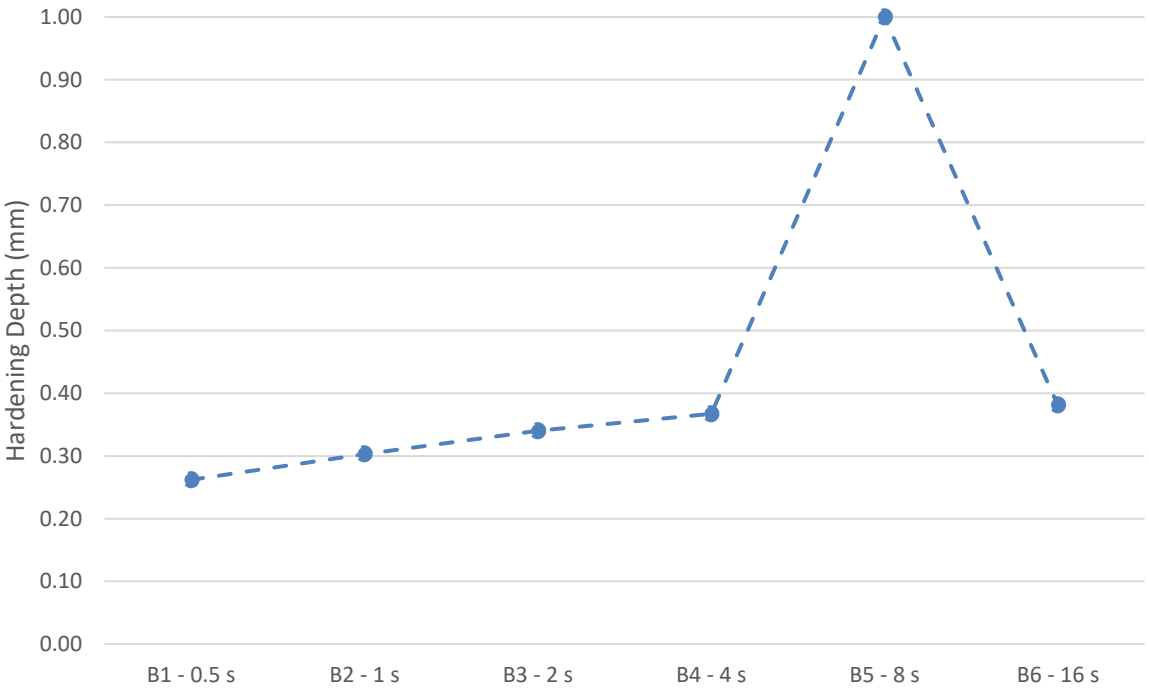

Figure 11- Influence of the interaction time on the hardening depth for laser hardened conventional hardened and tempered base specimens

Figures 12 and 13 represent the hardening depth profiles for the laser hardened specimens corresponding to the optimal process parameters, specimens A6 and B5, respectively. The hardening depth profiles for the remaining laser surface hardened specimens are available in Appendix II.

Starting by the analyzing the specimen A6 (figure 12), the hardened zone initiates at the surface, with a value of approximately 786 HV 0.3. Considering the hardness limit relative to the hardening depth of 625 HV as defined by the ISO 18203:2016 standard, the HZ extends until approximately 0.8 mm in depth. From this point on, the previously established transition zone begins. By considering the annealed state hardness of around 270 ± 5 HV 0.3 it is possible to determine that the

transition zone begins at around 0.8 mm in depth and ends at around 2.1 mm in depth. From this point onwards, the base material is achieved.

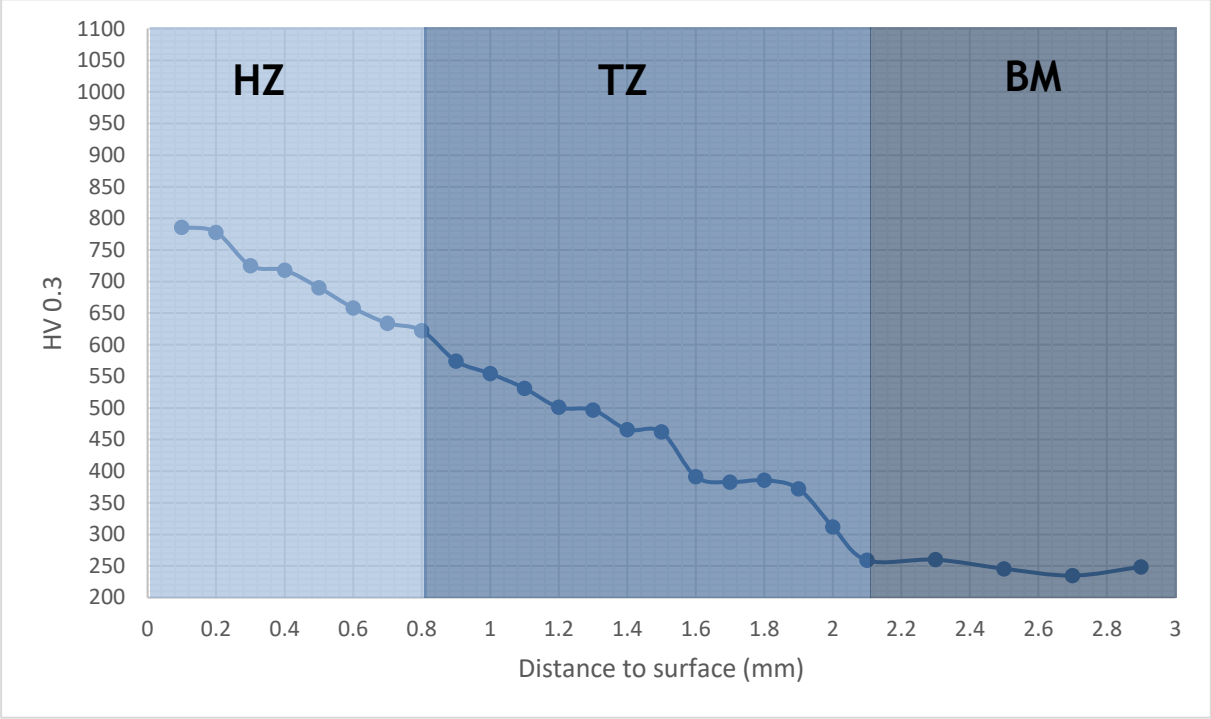

Figure 12- Hardening depth profile of the specimen A6, annealed base laser hardened with an interaction time of 16 seconds

By further exploring the transition zone of the specimen A6 (figure 12), it is possible to state that this microstructural region is characterized by presenting a larger volume of material when compared to the hardened zone. Furthermore, throughout the transition zone, it is expected to observe microstructural changes as depth increases, fact revealed by the large hardness dispersion. This continuous flow of change is the result of the different heat treatment conditions felt at different depths. In shallower areas, the heating and colling conditions are severe enough to promote the martensitic transformation, but in deeper areas, particular around the 1.6 mm in depth mark onwards, the heat treatment conditions aren't capable of promoting martensitic transformation, but instead, produce a finer annealed microstructure, an effect further explored on chapter 4.3. Microstructural Characterization.

For the specimen B5, laser hardened from conventional hardened and tempered base material (figure 13), the hardening depth is approximately 1.0 mm,

where the hardness reaches a value of 777 ± 10 HV 0.3. Such hardness value was defined as the hardness limit for the hardening depth, by conducting low-force Vickers hardness tests on the conventional hardened and tempered specimen without any kind of laser processing (specimen B0). At the closest region to the surface, the hardened zone presents a maximum hardness value of around 1012 ± 8 HV 0.3, value that goes hand to hand with the relative high surface hardness values obtained. The transition zone initiates at 1.0 mm in depth and ends at around 2.6 mm in depth, point from where the base material zone starts.

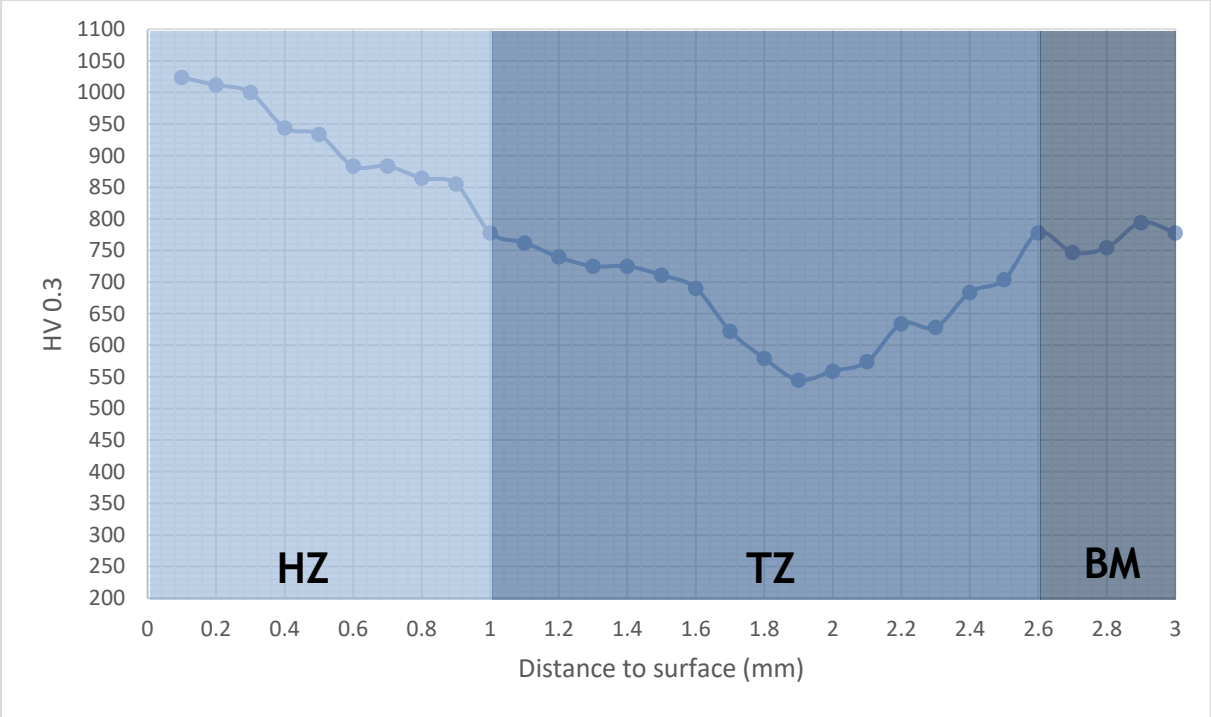

Figure 13- Hardening depth profile of the specimen B5, conventional hardened and tempered base laser hardened with an interaction time of 8 seconds

Once again, the transition zone is the microstructural area that presents the most pertinent variation as the distance to the surface increases. Similar to what is observed in the hardening depth profile of the specimen A6 (figure 12), the first hardness variation in the transition zone is characterized by a decrease in the hardness value. Such behavior is possibly a product of the lower heating and cooling conditions of this region, eventually producing increasingly coarser martensite microstructures as depth increases. Unlike the annealed base laser surface hardened specimen, the specimen B5 does not end this decrease in hardness with the beginning

of the base material region. Instead, an increase in the hardness value, around 1.9 mm in depth is observed, which extends to approximately 2.6 mm in depth. Such effect is closely related to the metallurgical condition of the base material, composed by tempered martensite. The heating and colling characteristics of this sub-region of the transition zone provides the occurrence of a tempering heat treatment. At around 1.9 mm, the tempering temperature is above the secondary hardening peak, thus minimal hardness is registered. From 1.9 mm until 2.6 mm the hardness value starts to increase. Such an effect is explained by the increasingly lower energy input provided by the laser as depth increases. In turn, a progressive decrease of tempering temperature is expected, until reaching a region where the laser action is null. It is from this point on that the base material hardness can be observed.

To sum up the harness analysis, there are some key notes to present. The first, and despite only two specimens from both base material groups, were considered as exhibiting the optimal process parameters, in the industrial environment, these process parameters may not be the preferred ones. This is because each component being developed/produced exhibits specific mechanical and metallurgical requirements to meet, where maximum surface hardness and/or hardening depth may not be required. Despite this fact, the construction of both surface hardness curves and hardening depth profiles provides the acquisition of a useful process window.

The second fact is relative to the surface hardness of the conventional hardened and tempered specimens (B family), where hardness values of around 69 ± 1 HRC or 1012 ± 8 HV 0.3, where achieved. Knowing that the martensite transformation requires the presence of carbon atoms available to accommodate the conversion from austenite to martensite, such high hardness values indicate a high level of “consumption” of carbon during this transformation [24]. The only negative aspect from this intense transformation is that the SAE M2 owes its high wear resistance not mainly to the martensite content but to the carbide content in its microstructure [38, 39]. If there is no available carbon to precipitate such carbides, MC, and M_6C, it should be expected that, despite the extremely high hardness value, the wear resistance will not follow the same pattern. As it will be demonstrated, these relatively high values of hardness were mitigated during the tempering heat

treatment. Nonetheless, it is important to mention that such high values of hardness may not be the best answer to the laser surface hardening process of the SAE M2.

4.2. Microstructural Characterization

The microstructural characterization was performed according to the principle of properly establishing all microstructural changes during laser surface hardening and the accurate identification of the microconstituents.

Beginning with the as-received annealed SAE M2 (specimen A0), figure 14 is an image of the specimen's A0 microstructure obtained via OM. First and foremost, and by comparison with bibliographic data [39, 60] regarding microstructures of annealed SAE M2, it is possible to identify a ferrite matrix (light gray background) with a large amount of disperse carbides (particles with dark outlines). The objective of such heat treatment is to produce a low-hardness microstructure, consisting of dispersed spheroidized carbides on a ferrite matrix. The carbide structure after annealing is usually composed by two types of carbides. Primary eutectic carbides formed during solidification and partially broken down by hot working, and secondary carbides. The secondary carbides, and as previously described on subchapter 2.3.1.1. Carbides, result from the decomposition of the M_2C metastable carbide to the MC and M_6C carbides. More so, the primary carbides usually present relatively larger dimensions when compared to the secondary carbides [39, 61]. By observation of figure 14, it is then possible to conclude that the large "blocky" carbides, marked as A, correspond to primary carbides and that the smaller spheroidized carbides, marked as B, more uniformly distributed throughout the microstructure and characterized by forming dark spots, correspond to secondary carbides.

Furthermore, and by resorting to the XRD graph of the as-received annealed state specimen, available in Appendix III, it is possible to conclude that the carbides present in the microstructure are the MC and M_6C, as the peaks of the XRD graph indicates. The XRD graph only reveals peaks of Fe α, which in the case of the annealed state, corresponds to the ferrite phase, and where, no peaks corresponding to the Fe γ and to the M_2C carbide were identified.

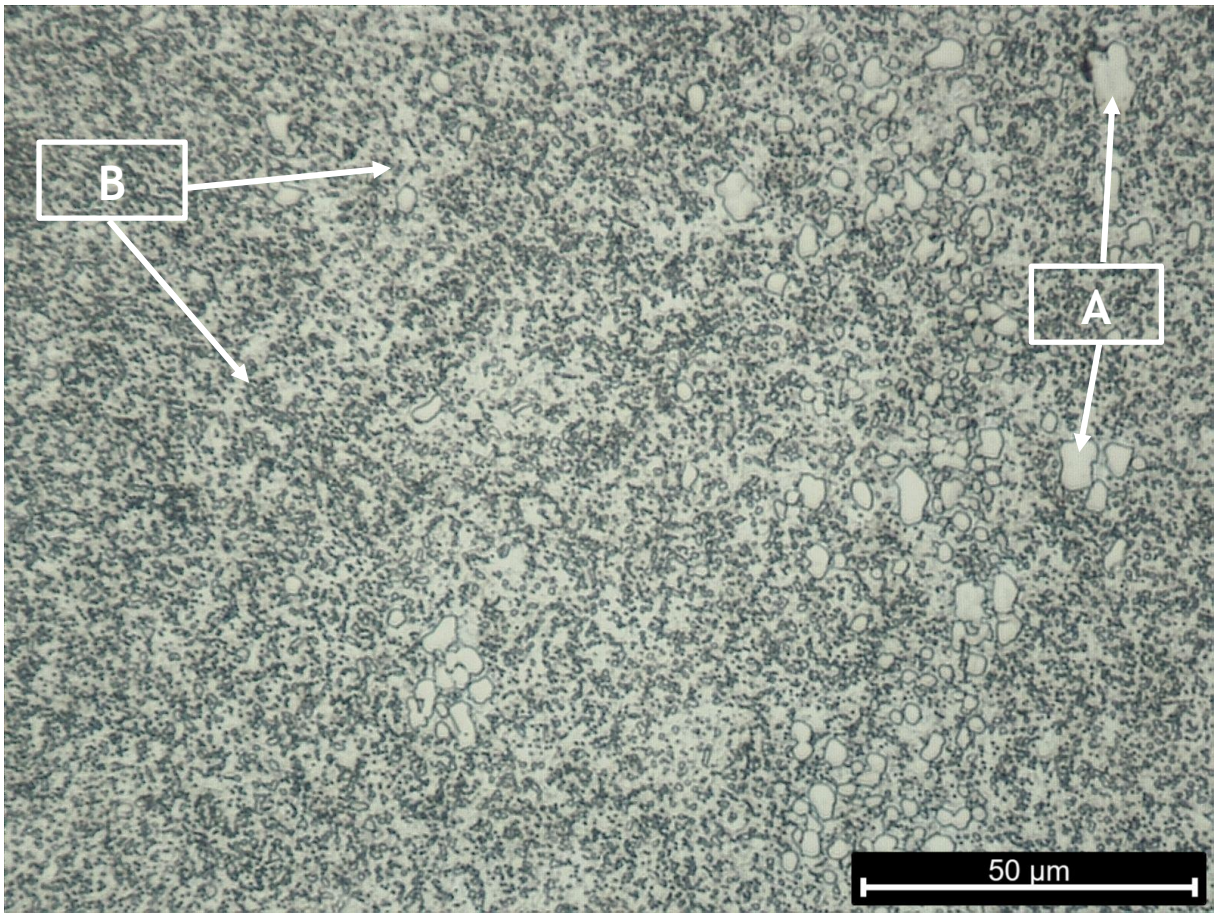

Figure 14– Microstructure of the as-received annealed SAE M2 via OM etched with a 2% Nital and 4% Picral mixture; A – Primary carbides; B- Secondary Carbides

To properly distinguish the MC carbide from the M_6C carbide in the microstructure, it is necessary to resort to higher magnifications, only reachable by SEM/EDS microscopy. By observation of figure 15, the two carbide types present in the annealed SAE M2 are easily identified. The carbide identified as 1 corresponds to the MC carbide (dark-grey particles), and the carbide 2 corresponds to the M_6C carbide (light-grey particles). The identification of both carbides is possible due to the semiquantitative analysis (table 7), where for carbide 1 a relative high vanadium content is observed, characteristic of the MC carbide. Meanwhile, the M_6C carbide is characterized by having a relative low vanadium content, phenomenon clearly identified during the analysis of carbide 2. More so, and similar to what was observed on the OM image (figure 14), it is possible to identify the primary carbides, that result from the initial as-cast microstructure, with larger dimensions, and the secondary carbides that result from the decomposition of the M_2C carbide, with relative smaller dimensions and rounder morphologies.

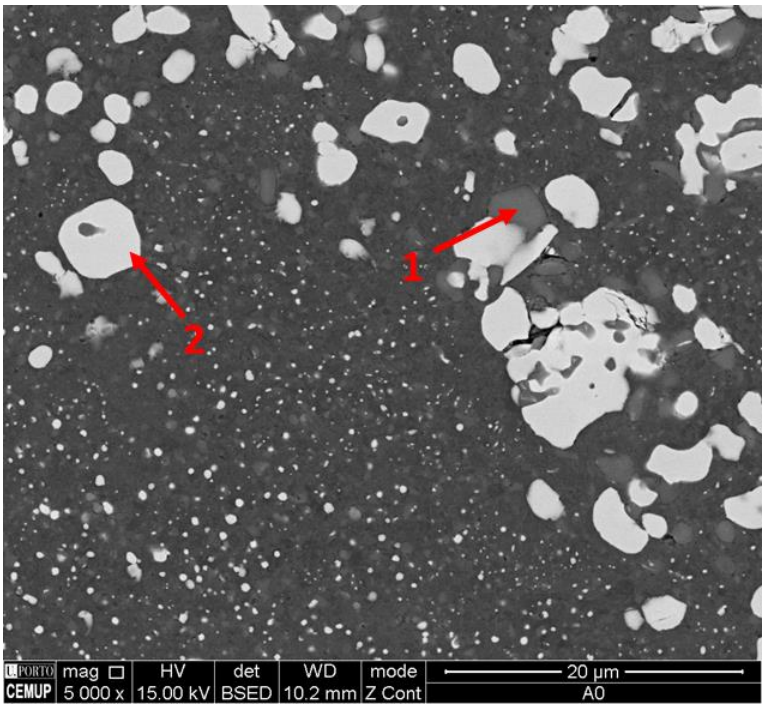

Figure 15– Microstructure of the as-received annealed SAE M2 via SEM/EDS; 1- MC carbide; 2- M_6C carbide

Table 7- Semiquantitative analysis of the as-received annealed SAE M2

	C	W	Mo	V	Cr	Fe
1	7.71	25.41	24.05	**30.96**	3.41	11.86
2	2.33	38.93	25.12	**2.50**	3.59	27.53

Values presented in weight percentage (wt %)

The annealed base laser surface hardened specimen with the previously established optimal process parameters (specimen A6) presents a cross-section composed by three distinct microstructural zones, as already exposed during the hardening depth analysis, subchapter 4.1.2. Figure 16 is a microstructural image of these three distinct regions, duly marked, and where the microstructural changes promoted by the laser heat treatment are evident. The hardened zone (HZ) is characterized by its location, the most superficial region, but also due to its darker coloration when compared to the transition zone.

Figure 16– Cross-section of the laser surface hardened annealed base specimen with an interaction time of 16 seconds (A6) etched with a 2% Nital and 4% Picral mixture

By resorting to figure 17, the hardened zone portrays a microstructure characteristic of a hardened SAE M2, composed by a martensitic matrix with large carbide precipitation. By comparing the microstructure of the annealed SAE M2 before (figure 14) and after (figure 17) laser surface hardening, the evolution from an annealed state, characterized by a ferritic matrix, to a quenched state is obvious. Nonetheless, the carbide structure remained similar even after laser surface hardening, being composed by primary (marked as A) and secondary (marked as B) carbides. Once again, such strong microstructural evolution demonstrates the hardening potential of the laser technology on the SAE M2.

Furthermore, and according to the SEM/EDS (figure 18) and semiquantitative analysis (table 8), two types of carbides are observed on the hardened zone. The MC (identified as 1, dark-grey particles) and the M_6C (identified as 2, light-grey particles). Lastly, and as expected, the XRD graph of the hardened zone for the specimen A6, available in Appendix III, presents peaks corresponding to the M_6C and MC carbide. No peaks regarding the Fe γ were identified, thus no retained austenite must be considered on the specimen A6.

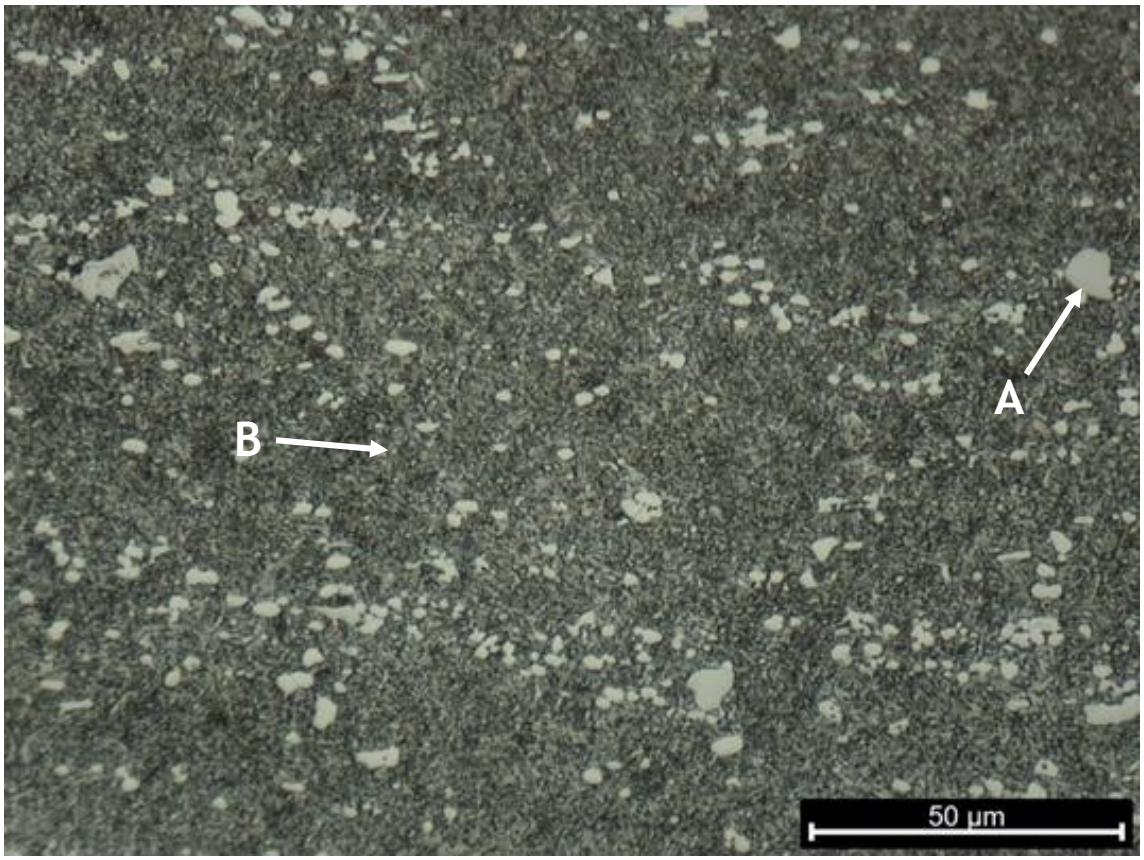

Figure 17- Microstructure of the hardened zone on the laser surface hardened annealed base specimen with an interaction time of 16 seconds (A6) via OM etched with a 2% Nital and 4% Picral mixture; A – Primary carbides; B- Secondary Carbides

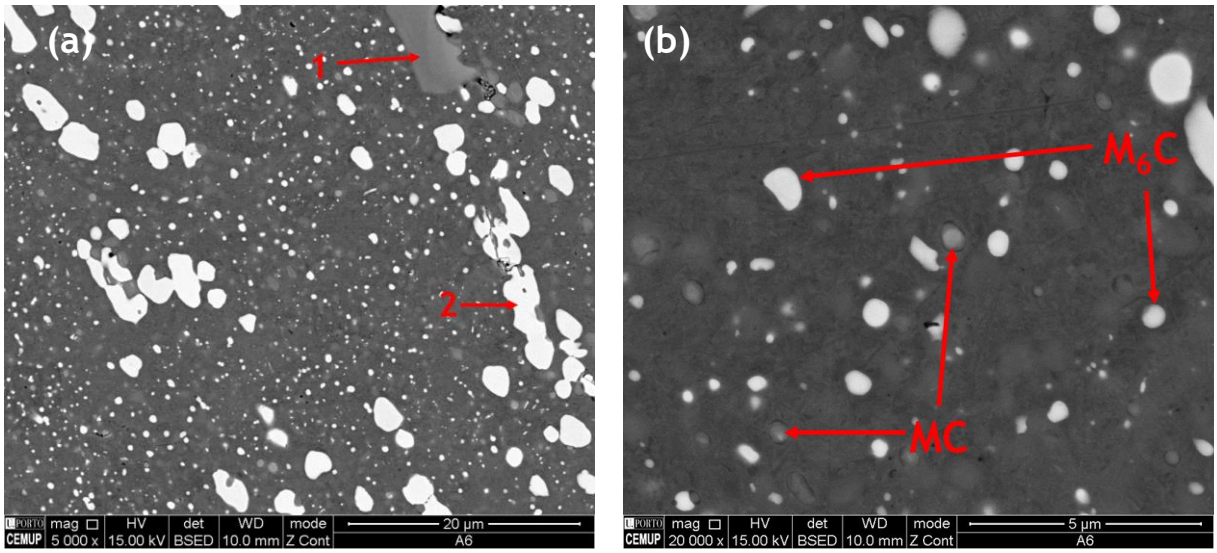

Figure 18- (a) and (b) Microstructure of the hardened zone of the laser surface hardened annealed base specimen with an interaction time of 16 seconds (A6) via SEM/EDS; 1- MC carbide; 2- M_6C carbide

Table 8- Semiquantitative analysis of hardened zone on the laser surface hardened annealed base specimen with an interaction time of 16 seconds (A6)

	C	W	Mo	V	Cr	Fe
1	6.15	28.41	17.09	**41.97**	3.43	2.95
2	1.64	39.04	24.12	**3.03**	3.57	28.61

Values presented in weight percentage (wt %)

By moving to deeper areas, relative to the surface, the microstructure begins to present characteristics of a partly austenitized and potential hardened structure. Such occurrence corresponds to the transition zone (figure 19 (a)). As previously described, this microstructural zone presents significant changes throughout its extension. In the upper areas of the transition zone, the heating and cooling conditions can promote the martensitic transformation. As depth increases, these same conditions are increasingly lower in intensity, promoting only a potentially finer annealed structure. On the other hand, the base material microstructure (figure 19 (b)) is equivalent to the microstructure of the as-received annealed specimen (figure 14), where as expected, the laser action does not promote any microstructural modifications. To conclude, all the observed microstructural changes throughout the different zones are an image to what was observed during the hardening depth analysis (subchapter 4.1.2.) of the specimen A6.

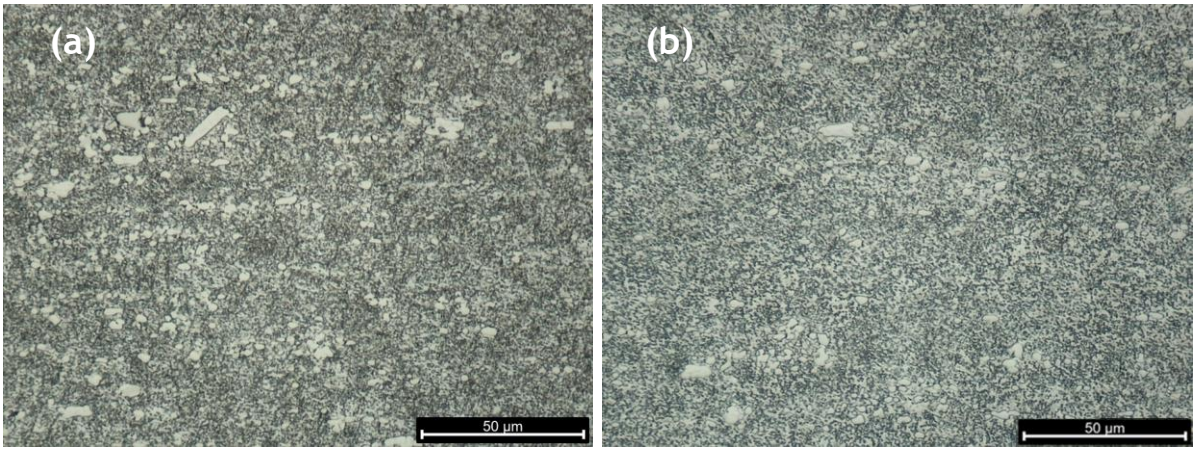

Figure 19- (a) Transition zone and (b) base material microstructures of the laser surface hardened annealed base specimen with an interaction time of 16 seconds (A6) via OM etched with a 2% Nital and 4% Picral mixture

The microstructure of the as-received conventional hardened and tempered SAE M2 (specimen B0) is presented in figure 20. By its observation, and resorting to bibliographic data [6, 9, 41, 48, 60], it is possible to identify a metallic matrix composed by tempered martensite with randomly distributed carbides (white particles). The primary carbides, marked as A, and with relative larger dimensions, appear distributed along the direction of previous hot work operations, and where the sequence of the conventional heat treatment wasn't capable of promoting its entire dissolution. On the other, the smaller and rounder carbides, marked as B, distributed more uniformly, are the combination of the precipitation during the annealing and hardening heat treatments and the secondary precipitation during tempering.

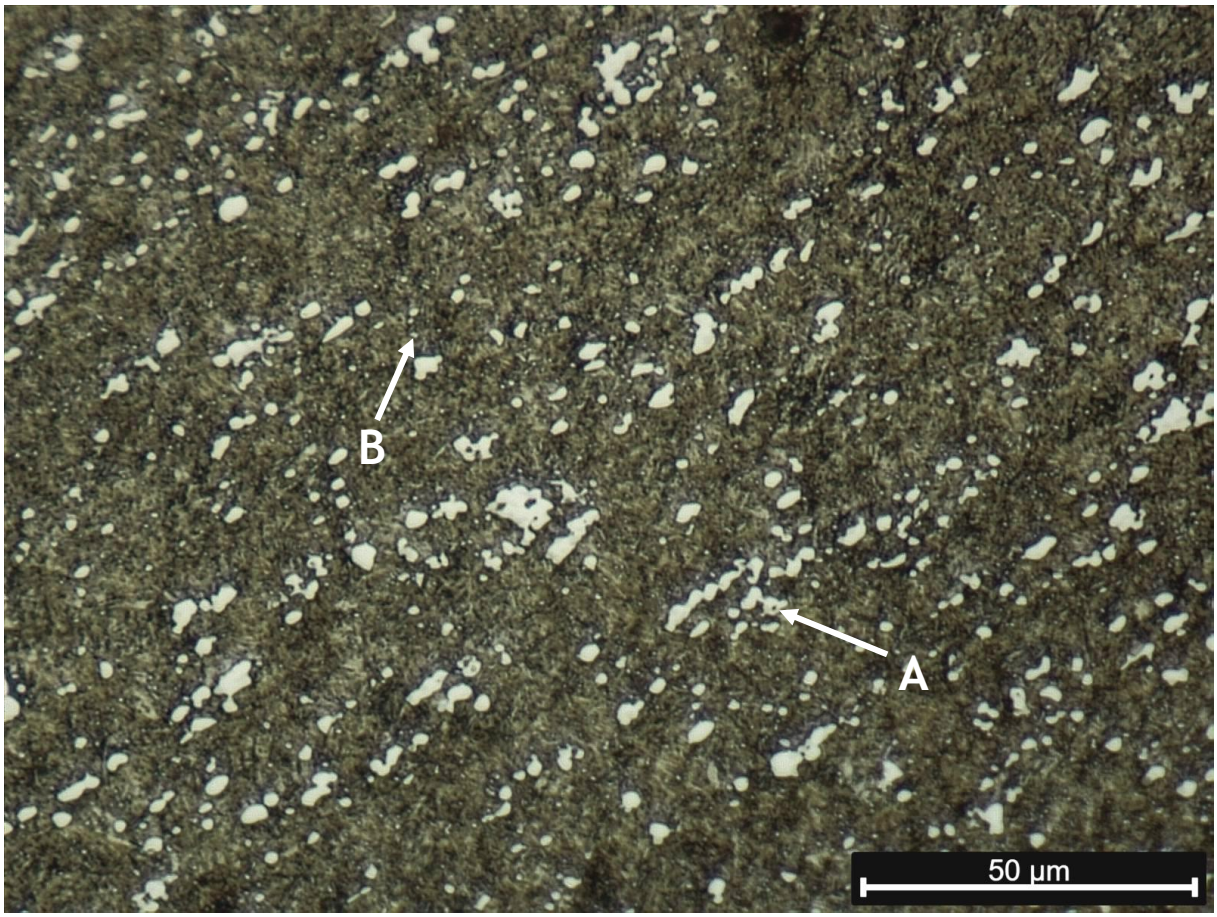

Figure 20- Microstructure of the as-received conventional hardened and tempered SAE M2 via OM etched with a 2% Nital and 4% Picral mixture; A- Primary carbides; B- Secondary Carbides

By resorting to higher magnifications (figure 21) and semiquantitative analysis (table 9), it is possible to identify the presence of both the MC and M_6C carbides in the microstructure. Such phenomenon is also identified on the XRD graph of the specimen B0, available in Appendix III, where peaks corresponding to both carbides are observed. No peaks regarding the Fe γ were detected, therefore no retained austenite is considered after conventional hardening and tempering heat treatment. Similar to what is observed in figure 20, the presence of both primary and secondary carbides is evident. As previously described, the primary carbides present larger dimensions when compared to the secondary carbides. As explained before, in this case, the secondary carbides derive from two different sources. They can result from the annealing and hardening heat treatments, and the tempering heat treatment, where secondary hardening via carbide precipitation is expected.

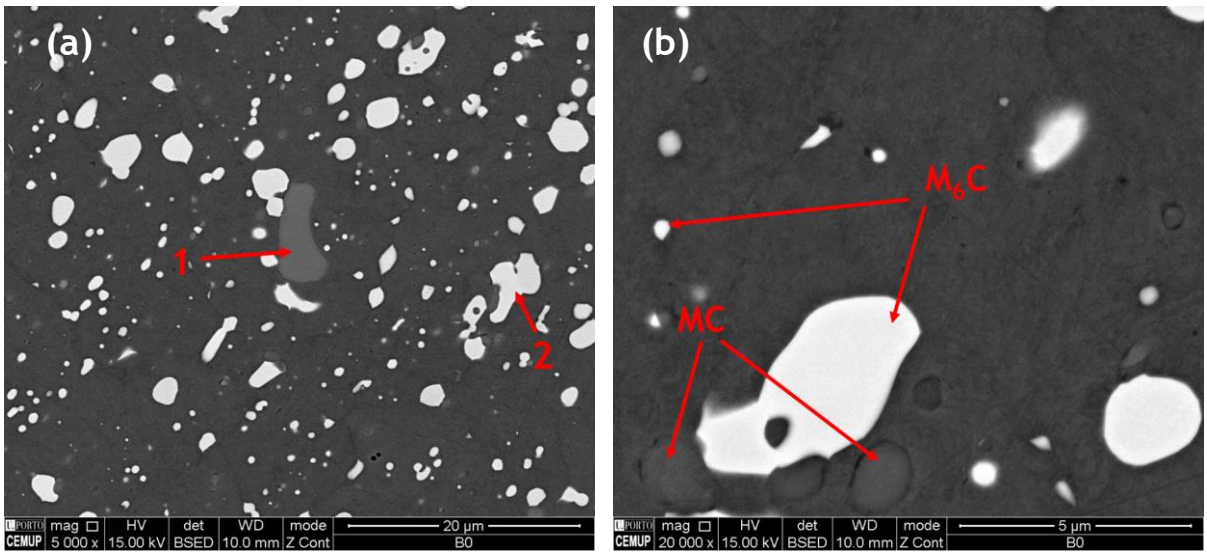

Figure 21- (a) and (b) Microstructure of the as-received conventional hardened and tempered SAE M2 via SEM/EDS; 1- MC carbide; 2- M_6C carbide

Table 9- Semiquantitative analysis of the as-received conventional hardened and tempered SAE M2

	C	W	Mo	V	Cr	Fe
1	6.57	26.66	16.19	**44.46**	3.39	2.74
2	1.42	36.94	25.71	**2.79**	3.87	29.28

Values presented in weight percentage (wt %)

Figure 22 represents an image of the cross-section of the conventional hardened and tempered base laser hardened specimen B5. Analogous to what is observed in figure 16 relative to the cross-section of specimen A6 and as expected, the cross-section of specimen B5 is divided into three separate regions: hardened zone, transition zone, and base material.

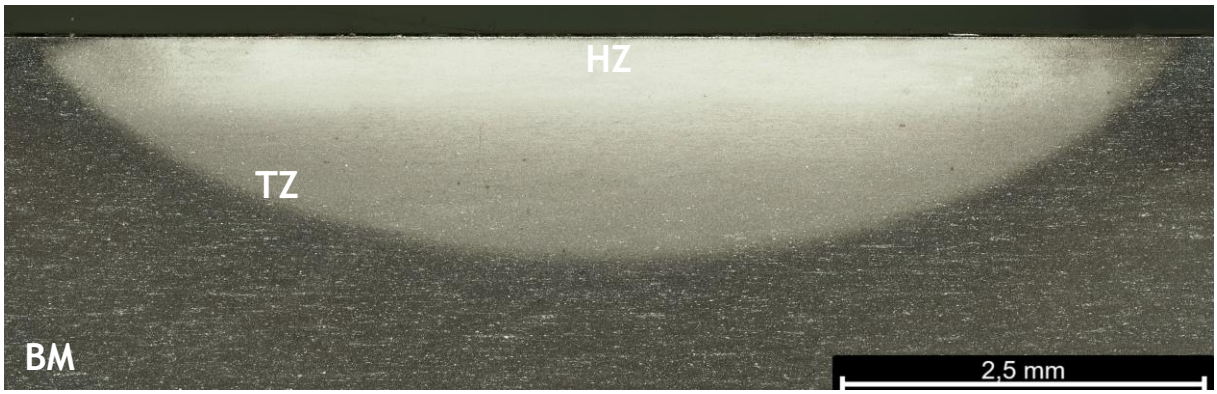

Figure 22- Cross-section of the laser surface hardened conventional hardened and tempered base specimen with an interaction time of 8 seconds (B5) etched with a 2% Nital and 4% Picral mixture

The hardened zone of the specimen B5 (figure 23) presents a microstructure that was not yet observed in any previous specimens discussed, characterized by a practically unetched matrix, despite the same etching conditions of the previous OM images. As described during hardness analysis, subchapter 4.1., this region presented unusually high hardness values. Such behavior was described as a result of the extreme conditions that this region was subjected during the laser heat treatment, and where a highly massive martensite was predicted. Consequently, and despite not being observed during OM analysis, a martensitic matrix with disperse carbides is established for the hardened zone. Furthermore, and considering the cross-section of the specimen B5 (figure 22), a progressive darker coloration of the microstructure is detected as depth increases, possibly a product of an increasingly coarser metallic matrix until reaching a tempered state, characteristic of the base material and where the effect of the laser process is null.

The carbides present in the hardened zone of the specimen B5 are the MC and M_6C, as identified by SEM/EDS analysis (figure 24) and semiquantitative results (table 10). Furthermore, the XRD graph of the same hardened zone (available in appendix III) also identifies the presence of both carbides. Similar to the hardened

zone of specimen A6, no peaks regarding the Fe γ were detected what concludes that no retained austenite is present on the hardened zone of the specimen B5.

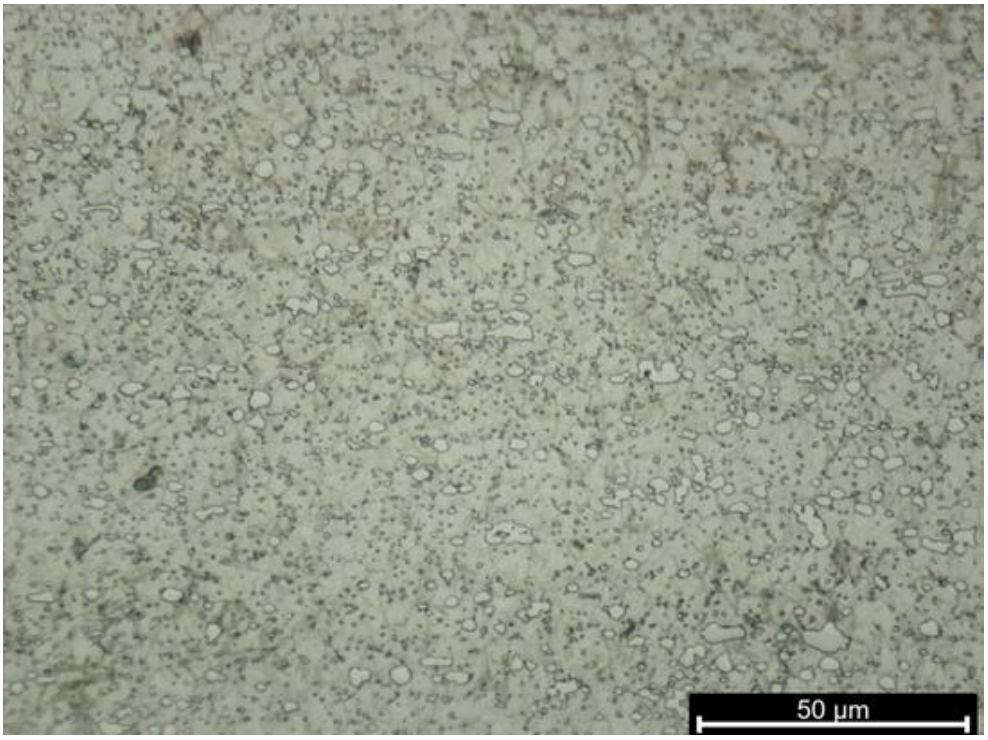

Figure 23– Microstructure of the hardened zone on the laser surface hardened conventional hardened and tempered base specimen with an interaction time of 8 seconds (B5) via OM etched with a 2% Nital and 4% Picral mixture

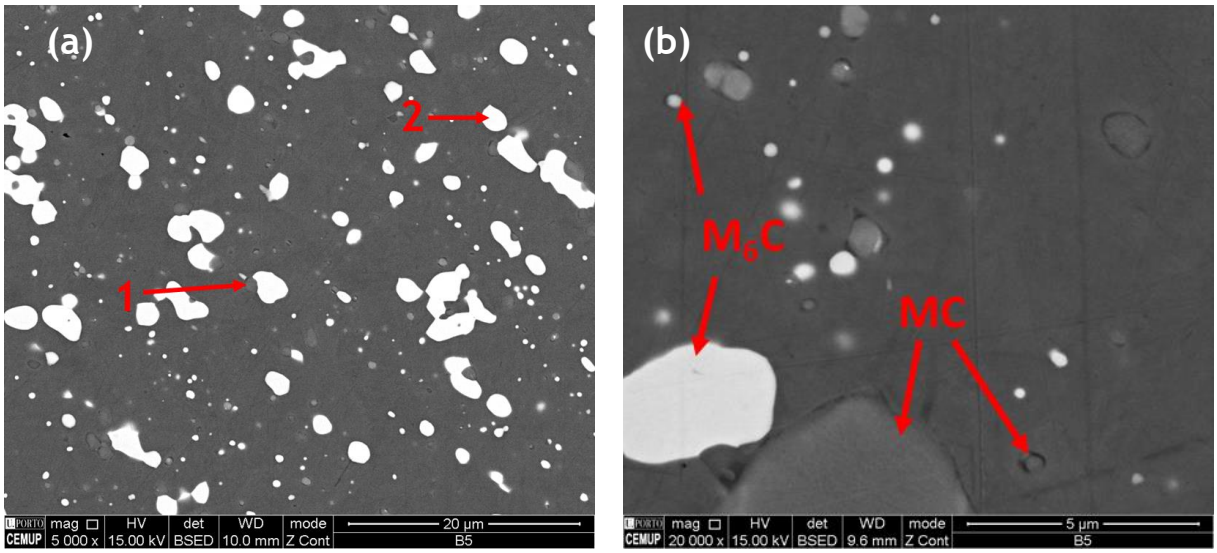

Figure 24- (a) and (b) Microstructure of the hardened zone of the laser surface hardened conventional hardened and tempered base specimen with an interaction time of 8 seconds (B5) via SEM/EDS; 1- MC carbide; 2- M_6C carbide

Table 10- Semiquantitative analysis of the hardened zone on the laser surface hardened conventional hardened and tempered base specimen with an interaction time of 8 seconds (B5)

	C	W	Mo	V	Cr	Fe
1	6.68	23.51	18.47	**39.18**	4.12	8.03
2	2.46	38.28	24.33	**2.60**	3.52	28.80

Values presented in weight percentage (wt %)

Regarding the transition zone and considering the microstructures obtained for such region (figure 25 (a) and (b)), it is possible to observe microstructural changes as depth increases. The superficial areas of the transition zone (figure 25 (a)) are characterized by presenting a lighter colored metallic matrix when compared to the deeper areas (figure 25 (b)). Furthermore, this evolution to a darker matrix continues until reaching the base material (figure 25 (c)), characterized by presenting a microstructure composed by tempered martensite and randomly disperse carbides. Following the above mention effect of matrix coloration on the microstructural characteristics, it is possible to conclude that the transition zone microstructure evolves from an eventually hardened microstructure, characterized by portraying a martensitic matrix, in the superficial areas to a tempered microstructure in the deeper areas. Additionally, no major changes in the carbide morphology are observed between the superficial areas (figure 25 (a)) and the deeper areas (figure 25 (b)) of the transition zone.

To conclude, the base material (figure 25 (c)) is characterized by presenting an equivalent microstructure to the as-received conventional hardened and tempered microstructure (figure 20), indicating that no metallurgical changes occurred during laser processing.

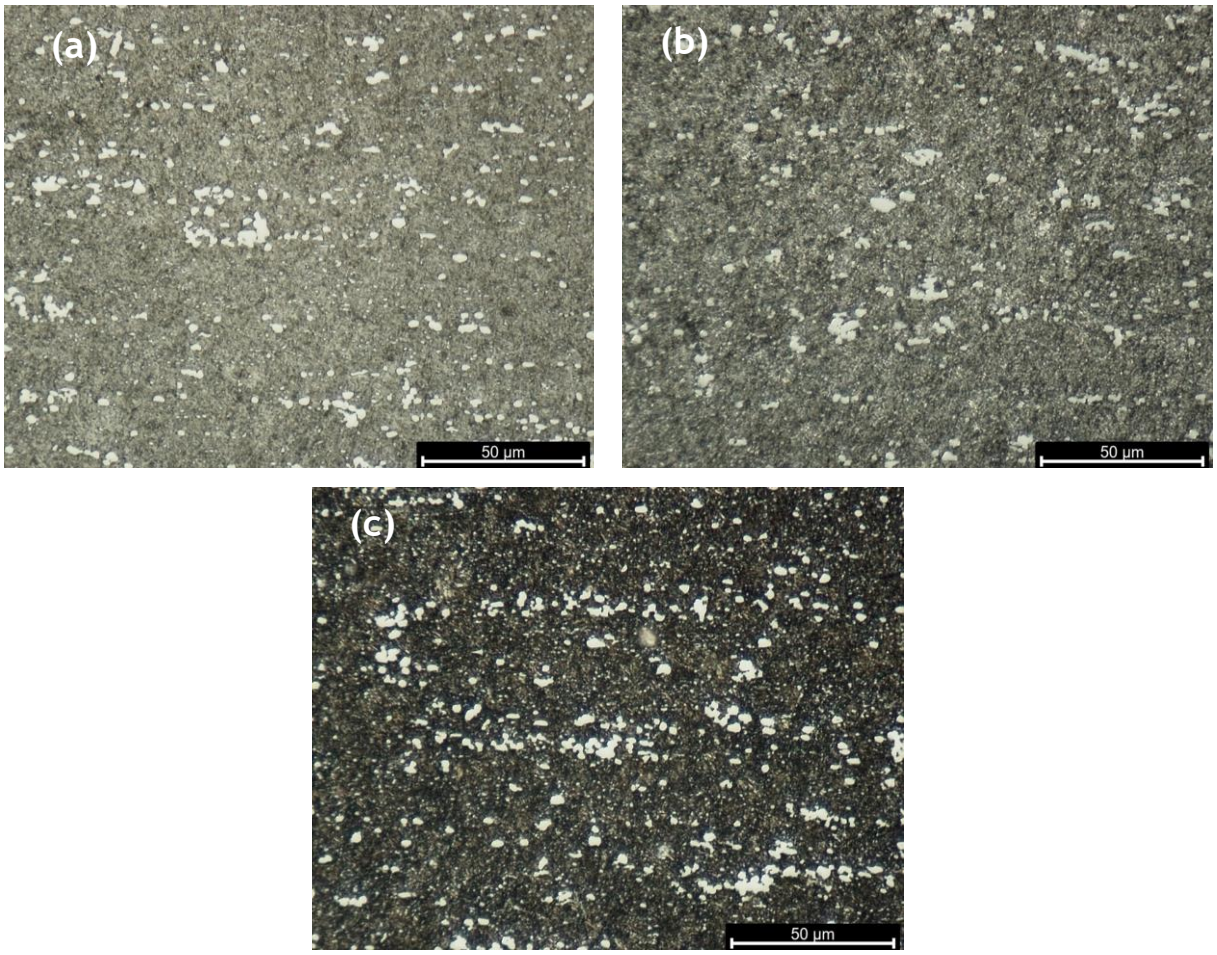

Figure 25– Transition zone, (a) superficial and (b) deeper areas; and (c) base material of the laser surface hardened conventional hardened and tempered base specimen with an interaction time of 8 seconds (B5) etched with a 2% Nital and 4% Picral mixture

4.3. Tempering Evaluation

To conclude the discussion of the experimental work conducted, an analysis of the tempering evaluation was performed. As previously described, such work had as primary intent the determination of possible changes in the tempering heat treatment behavior. This is due to the unique characteristics of the laser heat treatment, in what regards not only the extreme heat and cooling conditions but also the discrete region affected by such treatment.

In figure 26 the expected tempering curves for the different specimens produced are presented. The designation CH relates to the conventional heat treatment conducted on the annealed specimens which were, before the tempering

study, hardened by austenitizing at 1210 ºC and quenched in air. In the same figure, the curves of the laser hardened specimens, for both initial states of annealed and conventional hardened and tempered are also plotted. As described in subchapter 3.3. Tempering Evaluation, only the laser hardened specimens with the previously established optimal process parameters were analyzed (specimens A6 and B5).

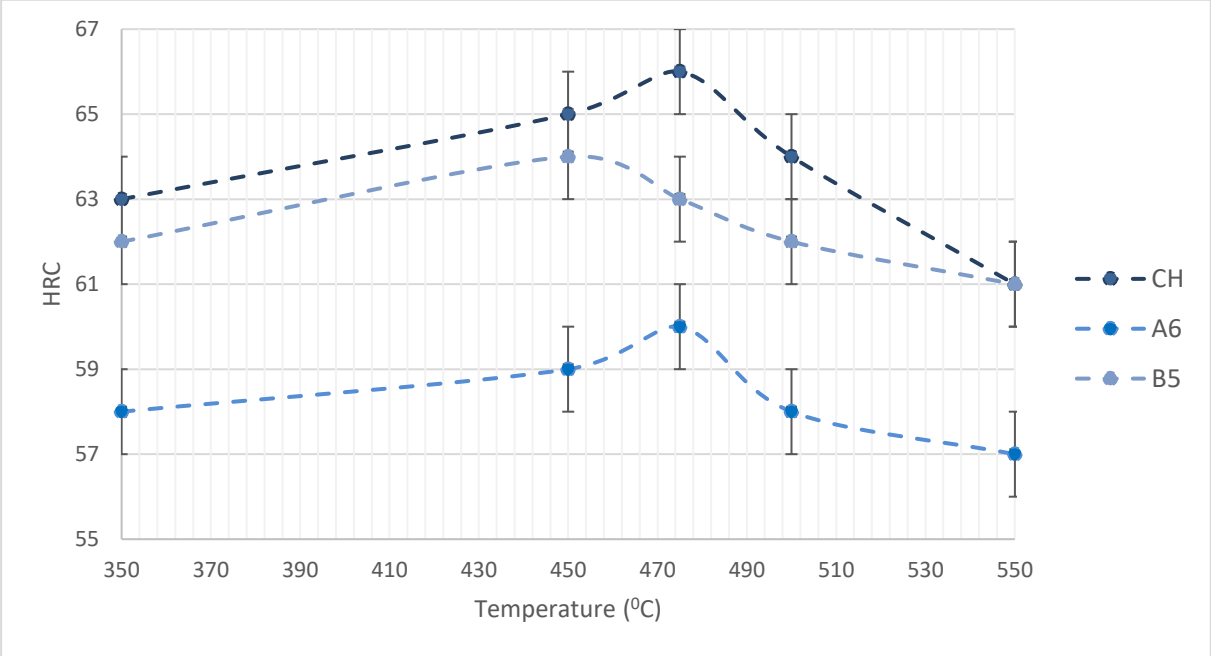

Figure 26- Comparison of the expected tempering curves between the conventional hardening treatment (CH), the laser surface hardened process conducted on an annealed base (A6) and the laser surface hardened process conducted on a conventional hardened and tempered base (B5)

By analysis of the expected tempering curve for the conventional heat treatment (CH) it becomes clear that secondary hardening peak occurs at 475 ºC. When comparing it with the tempering temperatures provided by different bibliographic sources [43, 59, 62-64], between 540 ºC and 595 ºC, the difference is obvious. This lower tempering temperature for maximum secondary hardening effect is possibly related to fluctuations on chemical composition upon production. More precisely, in the lower weight percentage of alloying elements, not providing such strong secondary hardening by carbide precipitation during the tempering stage. In any case, since the tempering evaluation is conducted based on a comparison method and that all the specimens were extracted from material that produced in the same batch, the variation of the temperature for secondary hardening peak should occur to all the analyzed specimens.

Moving forwards to the expected tempering curve of the specimen A6, and by comparison with the CH tempering curve, both curves present the same profile at different hardness levels. Both tempering curves present secondary hardening peak at around 475 ºC, where the CH curve presents an approximate hardness of 66 ± 1 HRC and the A6 curve a hardness around 60 ± 1 HRC. This movement of the tempering curve in the way of increasing/decreasing hardness is characteristic of variations in the austenitizing temperatures during hardening for HSSs. When the austenitizing temperature is increased, the tempered hardness values tend to rise to all the tempering temperatures (case of the CH curve). Such effect relates to the increased supersaturation of the as-quenched martensite, resulting in a more intense carbide precipitation during tempering [39]. The inverse phenomenon occurs when relatively lower austenitizing temperatures are employed, the case of the A6 curve. Just like what was discussed on the subchapter 4.1.1. Surface Hardness, the laser surface hardening process of the annealed base specimens should be explored in the way of exposing the material to longer interaction times, as the definition of the optimal process parameter of 16 seconds for interaction time is constrained by the pre-defined limits of the experiment itself. Nonetheless, the current analysis can demonstrate that the laser surface hardening process on the annealed state material produces a response to posterior tempering treatment in the same way as the conventional heat treatment does. Similar conclusions were taken by Shi *et al.* [8], who conducted a study on the influence of the preheat and post heat treatment on laser surface hardened SAE M2.

One other comparison study that can be conducted is between the hardness of the secondary hardening peak on specimen A6 and the hardness of the as-received conventional hardened and tempered SAE M2 (specimen B0), of 60 ± 1 HRC and 61 ± 1 HRC, respectively. The values are extremely close, supporting the idea that the laser surface hardening process on an annealed SAE M2 produces results that are an image to those of the conventional heat treatment, only differing on the size of the affected region.

To conclude, when considering the as-quenched hardness of the conventional hardened and the laser surface hardened annealed base specimens, of 66 ± 1 HRC and 60 ± 1 HRC respectively, both hardness' are kept after tempering at the temperature of secondary hardening peak. This behavior is very characteristic to

high-speed steels, where the tempering of the martensite, and consequently the lowering of hardness, is balanced by the secondary hardening effect and to some degree the transformation of any retained austenite. This transformation of retained austenite is the reason why a second and even triple tempering stage is recommended, as the recently transformed martensite is untempered resulting in lower toughness levels [39].

The expected tempering curve for the laser surface hardened conventional hardened and tempered base material, B5 on figure 26, presents a secondary hardening peak temperature slightly lower, around 450 ºC, then the previously observed at 475 ºC. When analyzing this behavior, it is necessary to consider that the overall heat treatment history for the specimen B5 is quite complex. First, a conventional hardening and tempering heat treatment, the last at 530 ºC, was conducted, followed by a laser hardening process and ending in tempering heat treatment. As previously mentioned numerous times, for this particular grades of steels, the heat treatment history will strongly define the mechanical properties of the material, where small changes to the temperatures and times are responsible for significant changes in, for example, the hardness value [5, 49]. Consequently, the complex heat treatment sequence of the specimen B5 may have led to changes on the secondary hardening peak temperature.

The secondary hardening peak for the B5 expected tempering curve displays a hardness of approximately 64 ± 1 HRC, representing a percentual increase of 5% compared to the conventional hardened and tempered base material from where the laser hardening process was conducted. On the other hand, if we compare the hardness value of the specimen B5 before tempering and after tempering at secondary hardening peak, a decrease of around 8% is observed. During the hardness analysis of the specimen B5, subchapter 4.1., such high levels of hardness were associated to a highly massive martensite formed during the laser hardening procedure, but where the possible negative effect on what regards carbide presence and distribution was mention. By performing the tempering heat treatment, such effect was possibly diminished, judging by the lower surface hardness.

Going back to the surface hardness analysis of the conventional hardened and tempered base laser hardened specimens, subchapter 4.1.1., a comparison between the laser hardened conventional hardened and tempered SAE M2, and the super

high-speed steels was conducted. With the hardness decrease after tempering such a phenomenon must be eliminated from the equation. Nonetheless, it is necessary to consider that the laser hardened specimens from the B family were processed on base material that presented relatively low values of hardness, around 61 ± 1 HRC. After laser surface hardening, a percentual increase of about 19% was observed. By conducting the same experiments on base material with higher surface hardness, such as the "in-house" produced conventional hardened and tempered specimens, higher surface hardness values could eventually be achieved. After tempering, such specimens could possibly fit onto the super high-speed steels category, eliminating the need to resort to more expensive HSS grades, such as the M42 [5].

Figure 27 and 28 are representatives of the hardening depth profiles of both laser hardened specimens with optimal process parameters in the as-quenched (A6 and B5 curves) and tempered (A6T and B5T), at the temperature of secondary hardening peak states. For the specimen A6, figure 27, the hardness variation between the as-quenched and tempered states are minimal, only occurring small changes in regions where the as-quenched hardness profile presented steep slopes. Such behavior is possible related to the stress-relieving effect of tempering [37]. It is then possible to conclude that the tempering heat treatment has a relatively small effect on the hardness distribution of the annealed base laser hardened SAE M2.

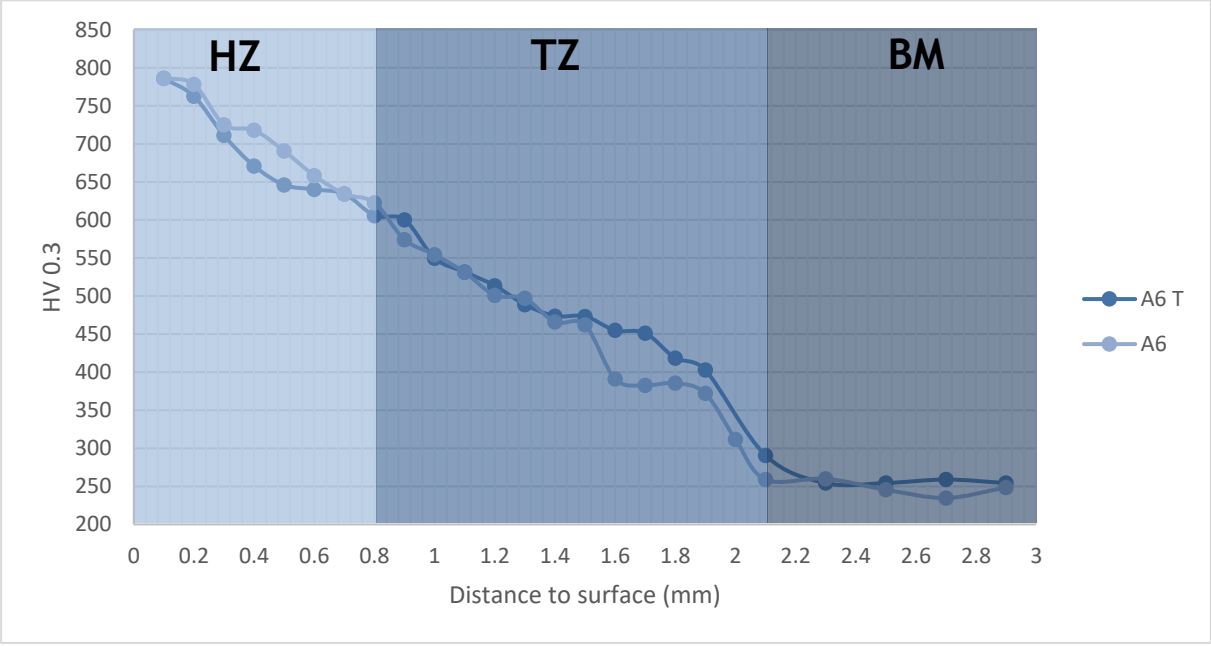

Figure 27- Hardening depth profiles of the specimen A6 for the as-quenched (A6) and tempered at 475 ºC (A6T) states

In the case of the specimen B5 (figure 28), the as-quenched state presented from the get-go unusually high hardness values at the surface, of around 1012 ± 8 HV 0.3. During the tempering heat treatment, all the previously established hardened zone, which extended from the surface to 1.0 mm in depth, presents a significant decrease in hardness to values around 810 ± 20 HV 0.3. Such a strong decrease, already established during the analysis of the expected tempering curves a few paragraphs above, is a product of the tempering heat treatment effect on the martensitic matrix. By resorting to figure 29, representative of the microstructure of the hardened zone on specimen B5 after tempering at 450 ºC, it is possible to observe a microstructure very similar to the microstructure of the as-received conventional hardened and tempered SAE M2 (figure 20 - specimen B0) composed by a tempered martensitic matrix and a significant carbide fraction. Such resemblances were not observed during the study of the as-quenched microstructure of the hardened zone on specimen B5 (figure 23), where a unique matrix morphology was observed. Nevertheless, and by resorting to the SEM/EDS images (figure 30), and the semiquantitative analysis (table 11), the carbide structure of the tempered specimen did not change compared to the as-quenched state (figure 24 and table 10), where MC and M_6C carbides are observed.

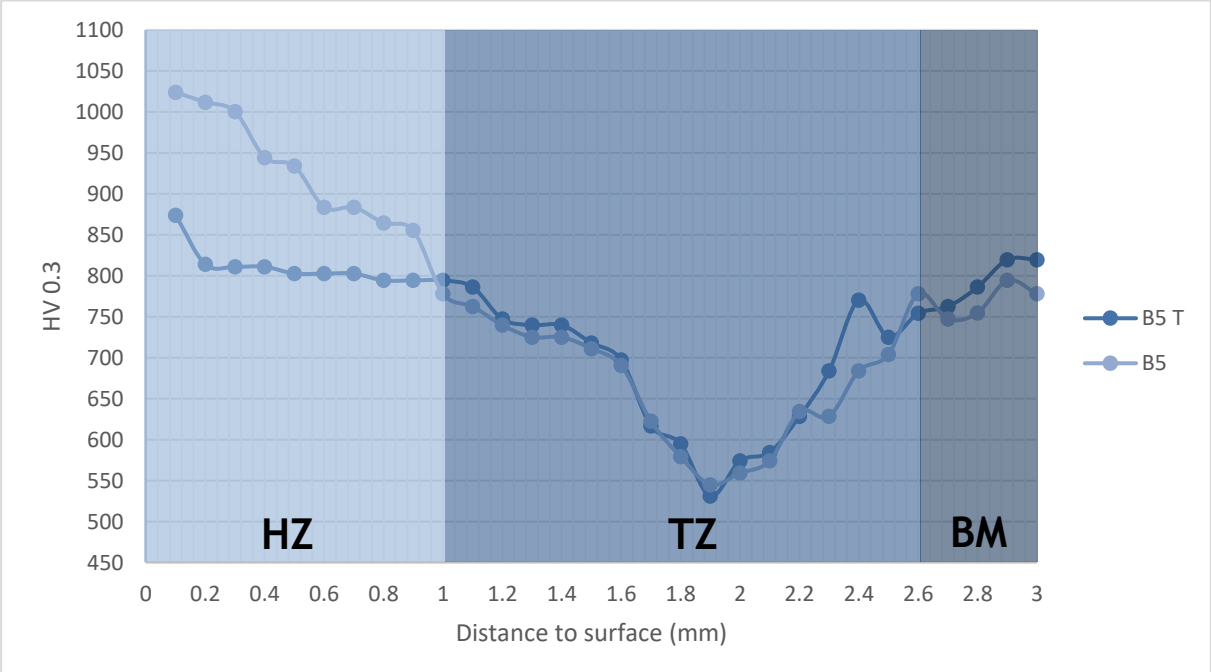

Figure 28- Hardening depth profiles of the specimen B5 for the as-quenched (B5) and tempered at 450 ºC (B5T) states

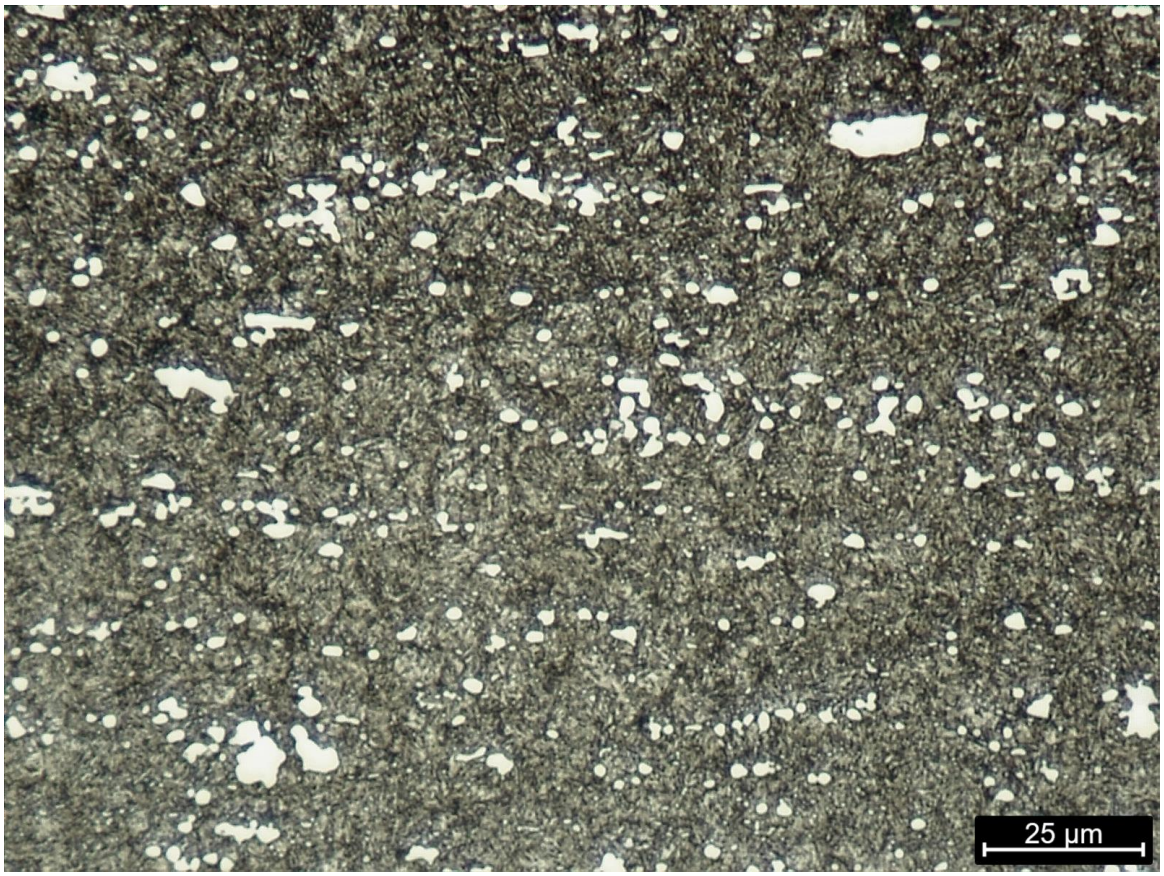

Figure 29– Microstructure of the hardened zone on the laser surface hardened B5 specimen, after tempering at 450 ºC via OM etched with a 2% Nital and 4% Picral mixture

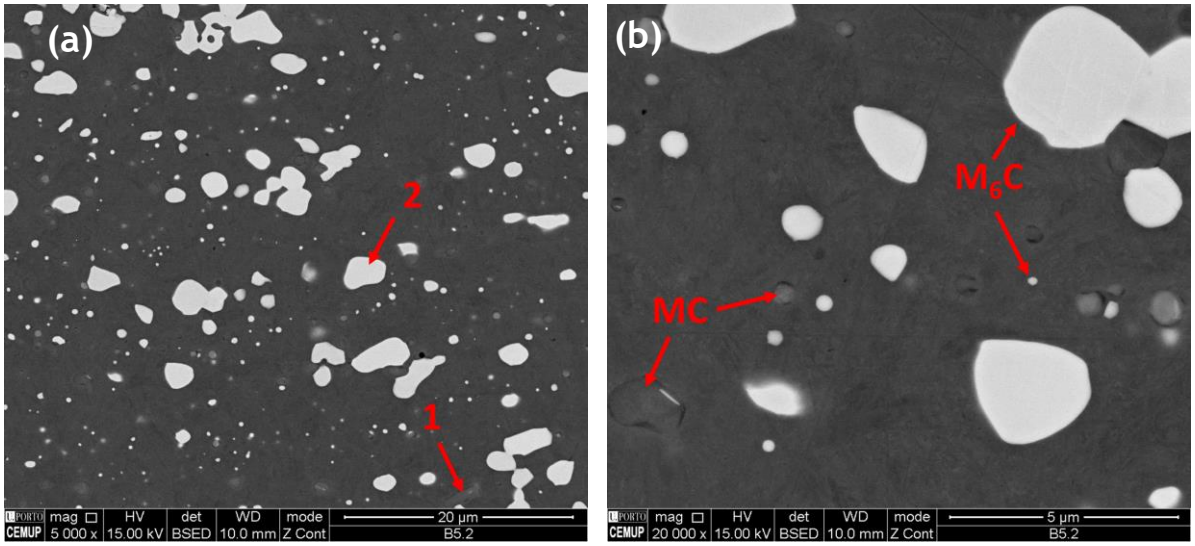

Figure 30- (a) and (b) Microstructure of the hardened zone on the laser surface hardened B5 specimen after tempering at 450 ºC via SEM/EDS; 1- MC carbide; 2- M_6C carbide

Table 11- Semiquantitative analysis of the hardened zone on the laser surface hardened B5 specimen after tempering at 450 ºC

	C	W	Mo	V	Cr	Fe
1	7.19	22.39	18.36	**41.11**	4.40	6.45
2	1.66	38.47	20.68	**2.03**	3.66	33.51

Values presented in weight percentage (wt %)

Despite the strong influence of the tempering heat treatment on the hardened zone, no major changes in the hardness distribution on the transition zone is observed (figure 28) for the conventional hardened and tempered base laser surface hardened specimen.

To conclude, on both annealed base and conventional hardened and tempered base laser surface hardened specimens (A6 and B5, respectively), the tempering heat treatment did not promote any change on the depth of the different microstructural zones, thus no change to hardening depth was observed after tempering.

5. Conclusions and Future Work

With the development of this work, it was possible to recognize the hardening potential of laser technology on the SAE M2, and understand the dynamic relationship between the process parameters and the resulting microstructural changes. More so, the use of two distinct initial microstructural states allowed for the analysis of the influence of the base material on the laser surface hardening process. Lastly, the execution of the tempering heat treatment on laser surface hardened material enables identifying any possible changes on the dynamics of such heat treatment promoted by the previous laser processing.

During laser surface hardening, two fixed process parameters were employed, with a third one, the interaction time being subjected to an optimization study. Surface temperature was set to 1290 ºC and a 10 mm square shape spot was defined.

For the annealed base laser surface hardened SAE M2 the interaction time of 16 seconds, representative of a 0.625 mm/s feed rate, provided the best response to the hardening operation. A surface hardness of 60 ± 1 HRC and a hardening depth of approximately 0.8 mm were determined. Meanwhile, the conventional hardened and tempered base laser surface hardened SAE M2 presented maximum surface hardness and hardening depth for an interaction time of 8 seconds, representative of a 1.25 mm/s feed rate. In this case, a surface hardness of 69 ± 1 HRC and a hardening depth of approximately 1.0 mm were obtained. In both cases, a considerable increase of the surface hardness was achieved compared to the base material hardness. All the laser hardened specimens presented a laser surface hardened layer for the different interaction times employed.

The study of the interaction time also demonstrated that for the annealed base specimens, the increase in the interaction time promoted an increase in both the surface hardness and the hardening depth. On the other hand, the interaction time influence on surface hardness for the conventional hardened and tempered base specimens did not follow the same pattern. For any given interaction time, the surface hardness presented a maximum value of around 69 HRC. The hardening depth for the conventional hardened and tempered specimens presented a behavior similar to what was observed for the annealed base specimens. The major difference between the two studies was that for the conventional hardened and tempered base

specimens an inflection point was reached, indicating a maximum reachable value of hardening depth during laser hardening. Such occurrences strongly support the idea that the previous microstructural state and heat treatment history of the base material present an enormous influence on the outputs of the laser hardening process.

The microstructural study of the above-mentioned optimal process parameter specimens as well as the base material specimens, demonstrated that for all of them, the carbides present were the MC and M_6C. In the case of the laser surface hardened specimens, their microstructure was composed by three distinct regions, these being, hardened zone, transition zone, and base material.

The experimental work was completed with the analysis of tempering on the laser surface hardened SAE M2. The tempering response of the laser surface hardened annealed base material is equivalent to the conventional heat treatment, only for different hardness levels. More so, the temperature of the secondary hardening peak was the same in both cases, of 475 ºC. On the other hand, the conventional hardened and tempered base laser surface hardened SAE M2 presents a significant decrease of surface hardness during tempering for a secondary hardening peak temperature of 450 ºC.

In the end, it is possible to conclude that laser surface hardening possesses the capability of producing equivalent hardened structures to those of the conventional heat treatment, and where higher wear resistance should be expected. More so, both the interaction time and the base material hold enormous influence on the resulting laser hardened microstructure and the overall properties of the hardened component.

Since no inflection was observed during the study of the annealed base laser surface hardened specimens in what regards surface hardness and hardening depth, longer interaction times should be explored. Furthermore, and aiming to clarify the impact of laser surface hardening on the performance during service, wear resistance tests should be conducted. Finally, despite not being mentioned throughout the work, the overlapping effect during laser surface hardening is a crucial phenomenon that needs to be properly studied and understood before its introducing to the market.

References

[1] J. Ion, *Laser Processing of Engineering Materials: Principles, Procedure and Industrial Application*. 2005.

[2] P. Dinesh, K. R. Balasubramanian, and G. Buvanashekaran, "Laser surface hardening: A review," *Int. J. of Surface Science and Engineering*, vol. 5, pp. 131-151, 2011.

[3] A. J. Elijah Kannatey, "Laser Surface Modification," in *Principles of Laser Materials Processing*, 2009, pp. 568-615.

[4] G. E. Totten, K. Funatani, and L. Xie, "Laser Surface Hardening," in *Handbook of Metallurgical Process Design*, New York: Dekker, 2004, pp. 641-731.

[5] R. A. Mesquita, K. Michael, and R. Schneider, "Tool steels : properties and performance," 2017.

[6] A. El-Batahgy, R. Ahmed, and A.-R. Moussa, "Laser Surface Hardening of Tool Steels—Experimental and Numerical Analysis," *Journal of Surface Engineered Materials and Advanced Technology*, vol. 03, pp. 146-153, 2013.

[7] A. I. H. Committee, "Surface Hardening of Steel," in *ASM Handbook, Volume 04 - Heat Treating*: ASM International, 1991.

[8] G. Shi, P. Ding, J. Liu, H. Yin, and J. Wang, "Microstructure and properties of laser surface hardened M2 high speed steel," *Acta Metallurgica et Materialia*, vol. 43, no. 1, pp. 217-223, 1995.

[9] F. B. Weina Liu, Dongyun Zhang, Ling Chen, Jingyi Wang, Yang Xia, "Laser surface hardening for tooling high-speed steel," *Laser Processing of Materials and Industrial Applications II*, 1998.

[10] W. M. Steen and J. Mazumder, "Background to Laser Design and General Applications," in *Laser Material Processing*, London: Springer London, 2010, pp. 11-78.

[11] A. J. Elijah Kannatey, "Laser Generation," in *Principles of Laser Materials Processing*, 2009, pp. 1-25.

[12] O. Svelto, "Introductory Concepts," in *Principles of Lasers*, Boston, MA: Springer US, 2010, pp. 1-13.

[13] A. J. Elijah Kannatey, "Laser Pumping," in *Principles of Laser Materials Processing*, 2009, pp. 63-70.

[14] J. Hecht, *Understanding lasers : an entry-level guide*. Piscataway, NJ; Hoboken, N.J.: IEEE Press ; John Wiley & Sons, 2008.

[15] L. Rofin-Sinar, *Introduction to industrial laser materials processing*. Hamburg, Germany: Rofin-Sinar Laser, 2000.

[16] D. F. Farson, J. F. Ready, and T. Feeley, *LIA Handbook of Laser Materials Processing*. Orlando: Laser Institute of America, 2001.

[17] J. L. Dossett and G. E. Totten, "34. Laser Surface Hardening," in *ASM Handbook, Volume 04A - Steel heat Treating Fundamentals and Processes*: ASM International, 2013.

[18] E. Kennedy, G. Byrne, and D. N. Collins, "A review of the use of high power diode lasers in surface hardening," *Journal of Materials Processing Technology*, vol. 155-156, pp. 1855-1860, 2004.

[19] J. L. Dossett and G. E. Totten, "34.3 Absorptivity," in *ASM Handbook, Volume 04A - Steel heat Treating Fundamentals and Processes*: ASM International, 2013.

[20] J. R. Davis, "10. Surface Hardening by Applied Energy," in *Surface Hardening of Steels - Understanding the Basics*: ASM International, 2002.

[21] G. Krauss, "21. Surface Hardening," in *Steels - Processing, Structure, and Performance*: ASM International, 2005.

[22] A. K. Nath and S. Sarkar, "Chapter 11 - Laser Transformation Hardening of Steel," in *Advances in Laser Materials Processing (Second Edition)*, J. Lawrence, Ed.: Woodhead Publishing, 2018, pp. 257-298.

[23] J. Prohaszka, "Phase transformations in steel during rapid heat treatment," vol. 32, pp. 87-96, 1988.
[24] P. M. Kelly, "1 - Crystallography of martensite transformations in steels," in *Phase Transformations in Steels*, E. Pereloma and D. V. Edmonds, Eds.: Woodhead Publishing, 2012, pp. 3-33.
[25] R. E. Smallman and A. H. W. Ngan, "Chapter 12 - Steel Transformations," in *Modern Physical Metallurgy (Eighth Edition)*, R. E. Smallman and A. H. W. Ngan, Eds. Oxford: Butterworth-Heinemann, 2014, pp. 473-498.
[26] G. Krauss, "4 - Physical metallurgy of steels," in *Automotive Steels*, R. Rana and S. B. Singh, Eds.: Woodhead Publishing, 2017, pp. 95-111.
[27] P. Dinesh, G. Buvanashekaran, and K. R. Balasubramanian, "Experimental studies on the microstructure and hardness of laser transformation hardening of low alloy steel," *Transactions of the Canadian Society for Mechanical Engineering*, vol. 36, pp. 241-257, 2012.
[28] S. Balasubramanian, V. Muthukumaran, and P. Sathyabalan, "A study on the effect of process parameters of laser hardening in carbon steels," *International Journal of Civil Engineering and Technology*, vol. 8, pp. 201-207, 2017.
[29] N. Barka and A. El Ouafi, "Effects of Laser Hardening Process Parameters on Case Depth of 4340 Steel Cylindrical Specimen—A Statistical Analysis," *Journal of Surface Engineered Materials and Advanced Technology*, vol. 5, pp. 124-135, 2015.
[30] M. Seifert, "Recent advances on laser based surface hardening technologies," F. IWS, Ed., ed. Dresden, Germany, 2018.
[31] S. Bonß, "Integration of laser beam hardening in high performance turning machines," Fraunhofer IWS, Dresden, Germany, 2008.
[32] A. J. Elijah Kannatey, "Background on Laser Processing," in *Principles of Laser Materials Processing*, 2009, pp. 407-430.
[33] A. J. Elijah Kannatey, "Laser Surface Modification," in *Principles of Laser Materials Processing*, 2008, pp. 568-615.
[34] L. S. Kremnev, "From high-speed tungsten steel to high-temperature molybdenum steel: A century of high-speed steel," *Steel in Translation*, vol. 39, no. 12, pp. 1111-1118, 2009.
[35] D. F. Heaney, "14.3.1 High-Speed Steels (HSSs)," in *Handbook of Metal Injection Molding (2nd Edition)*: Elsevier, 2019.
[36] B.-l. Liu, Z.-q. Lü, W.-w. Feng, T.-z. Ren, and W.-t. Fu, "Precipitation and decomposition behaviors of carbides in AISI M2 high-speed steel with nitrogen and mischmetal," *Journal of Central South University*, vol. 24, no. 4, pp. 782-788, 2017.
[37] A. M. Bayer and B. A. Becherer, "High-Speed Tool Steels," in *Machining*: ASM International, 1989, p. 0. Accessed: 2/19/2020.
[38] R. Komanduri, "Cutting-tool Materials," in *Encyclopedia of Materials: Science and Technology*, K. H. J. Buschow *et al.*, Eds. Oxford: Elsevier, 2001, pp. 1-13.
[39] G. Roberts, G. Krauss, and R. Kennedy, "14. High Speed Steels," in *Tool Steels (5th Edition)*: ASM International, 1998.
[40] A. M. Adaskin, "Applicability of P6M5 steel," *Russian Engineering Research*, vol. 30, no. 2, pp. 186-189, 2010.
[41] A. S. Chaus, "Structural and phase changes in carbides of the high-speed steel upon heat treatment," *The Physics of Metals and Metallography*, vol. 117, no. 7, pp. 684-692, 2016.
[42] M. Boccalini and H. Goldenstein, "Solidification of high speed steels," *International Materials Reviews*, vol. 46, pp. 92-115, 2001.
[43] *ASTM A600-92a(2016)-Standard Specification for Tool Steel High Speed*, ASTM, West Conshohocken, PA, 2016.
[44] X.-f. Zhou, D. Liu, W.-l. Zhu, F. Fang, Y.-y. Tu, and J.-q. Jiang, "Morphology, microstructure and decomposition behavior of M2C carbides in high speed steel," *Journal of Iron and Steel Research, International*, vol. 24, no. 1, pp. 43-49, 2017.

[45] M. M. Serna and J. L. Rossi, "MC complex carbide in AISI M2 high-speed steel," *Materials Letters*, vol. 63, no. 8, pp. 691-693, 2009.
[46] A.-M. Elrakayby and B. Mills, "Identification of carbides in high-speed steels," *Journal of Materials Science Letters*, vol. 5, no. 3, pp. 332-334, 1986.
[47] J. Jaworski, R. Kluz, and T. Trzepieciński, "Influence of Heat Treatment on Content of the Carbide Phases in the Microstructure of High-Speed Steel," *Archives of Foundry Engineering*, vol. 17, pp. 59-62, 2017.
[48] M. Serna, E. Jesus, E. Galego, L. Martinez, H. Correa, and J. Rossi, "An Overview of the Microstructures Present in High-Speed Steel-Carbides Crystallography," *Materials Science Forum*, vol. 530, p. 48, 2006.
[49] W. E. Bryson, "10. Heat Treating M2 High Speed Tool Steel," in *Heat Treatment, Selection, and Application of Tool Steels (2nd Edition)*: Hanser Publishers, 2009.
[50] M. Stoicanescu, E. Ene, A. Zara, I. Giacomelli, and A. Crisan, "The Heat Treatment Influence of 1.3343 High Speed Steel on Content of Residual Austenite," *Procedia Technology*, vol. 22, pp. 161-166, 2016.
[51] M. N. Kryanina, A. M. Bernshtein, and T. P. Chuprova, "Heat treatment of high-speed steel with continuous laser," *Metal Science and Heat Treatment*, vol. 31, no. 10, pp. 728-734, 1989.
[52] J. Kusiński, "Microstructure, chemical composition and properties of the surface layer of M2 steel after laser melting under different conditions," *Applied Surface Science*, vol. 86, no. 1, pp. 317-322, 1995.
[53] S. Kąc and J. Kusiński, "SEM and TEM microstructural investigation of high-speed tool steel after laser melting," *Materials Chemistry and Physics*, vol. 81, no. 2, pp. 510-512, 2003.
[54] C. T. Kwok, F. T. Cheng, and H. C. Man, "Microstructure and corrosion behavior of laser surface-melted high-speed steels," *Surface and Coatings Technology*, vol. 202, no. 2, pp. 336-348, 2007.
[55] K. Y. Benyounis, O. M. Fakron, and J. H. Abboud, "Rapid solidification of M2 high-speed steel by laser melting," *Materials & Design*, vol. 30, no. 3, pp. 674-678, 2009.
[56] J. Arias, M. Cabeza, G. Castro, I. Feijoo, P. Merino, and G. Pena, "Microstructure and mechanical behavior of laser surface melted AISI M2 high-speed steel," *Surface and Interface Analysis*, vol. 42, no. 6-7, pp. 752-756, 2010.
[57] M. Newishy, H. Abdel-Aleem, M. R. Elkousy, I. El Mahallawi, and A. El-Batahgy, "Surface treatment of AISI M2 tool steel by laser melting," *Key Engineering Materials*, vol. 786, pp. 128-133, 2018.
[58] M. Seifert, K. Anhalt, C. Baltruschat, S. Bonss, and B. Brenner, "Precise temperature calibration for laser heat treatment," presented at the AMA Conferences 2013, 2013.
[59] M. Bauccio, "6. Tool Materials," in *ASM Metals Reference Book (3rd Edition)*: ASM International, 1993.
[60] J. R. Davis, "42. Microstructural Analysis of Tool Steels," in *ASM Specialty Handbook Tool Materials*: ASM International, 1995.
[61] A. S. Chaus, A. V. Maksimenko, N. N. Fedosenko, Ĺ. Čaplovič, and V. N. Myshkovets, "Formation of Structure of an Annealed High-Speed Steel upon Laser Surface Melting," *Physics of Metals and Metallography*, vol. 120, no. 4, pp. 371-377, 2019.
[62] P. K. Samal and J. W. Newkirk, "51.4 Heat Treating Results by Example of AISI M2," in *ASM Handbook, Volume 7 - Powder Metallurgy (2015)*: ASM International, 2015.
[63] J. L. Dossett and G. E. Totten, "24. Heat Treating of High-Speed Tool Steels," in *ASM Handbook, Volume 04D - Heat Treating of Irons and Steels*: ASM International, 2014.
[64] G. Totten, "11. Tool Steels," in *Steel Heat Treatment Handbook*: CRC Press, 2006.
[65] J. Arias, M. Cabeza, G. Castro, I. Feijoo, P. Merino, and G. Pena, "Microstructural characterization of laser surface melted AISI M2 tool steel," *Journal of Microscopy*, vol. 239, no. 3, pp. 184-193, 2010.

Appendix

I. Previous Laser Hardening and Melting Studies on SAE M2

Authors	Setup				
	Output Power (W)	Feed Rate (mm/s)	Spot size (mm)	Laser System	
Shi *et al.* 1995 [8]	1500	----	3	CO_2	Laser Hardening
Liu *et al.* 1998 [9]	1200 ; 1400; 1800	17 ; 20 ; 25 ; 30	5 ; 6	CO_2	
El-Batahgy *et al.* 2013 [6]	400 ; 800 ; 1200 ; 1600 ; 1800	8.3 ; 16.7 ; 33.3 ; 66.7	1 ; 2 ; 3 ; 4	Nd:YAG	
Kryanina *et al.* 1989 [51]	----	----	-----	CO_2	Laser Melting
Kusinski 1995 [52]	----	0.42 – 33.3	----	CO_2 and Nd:YAG	
Kac *et al.* 2003 [53]	1330 ; 1850	13.3 ; 26.6	2 ; 3	CO_2	
Kwok *et al.* 2007 [54]	900	25	6	Nd:YAG	
Benyounis *et al.* 2009 [55]	30 ; 40 ; 60	0.5 ; 1 ; 2	0.5	Nd:YAG	
Arias *et al.* 2010 [56]	2000	25 ; 60	3 ; 6	Nd:YAG	
Newishy *et al.* 2018 [57]	600 ; 1000 ; 1400 ; 1800	8.3 ; 16.7	2 ; 4	Nd:YAG	

II. Hardening Depth Profiles

Specimen A1

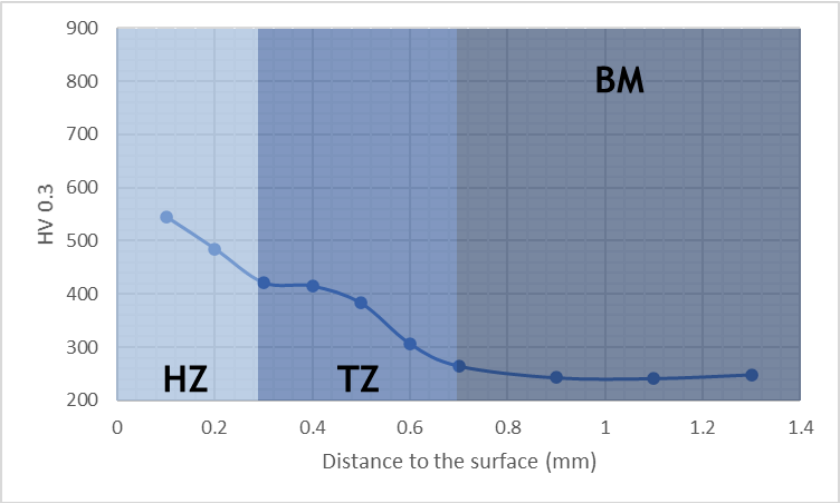

Specimen A2

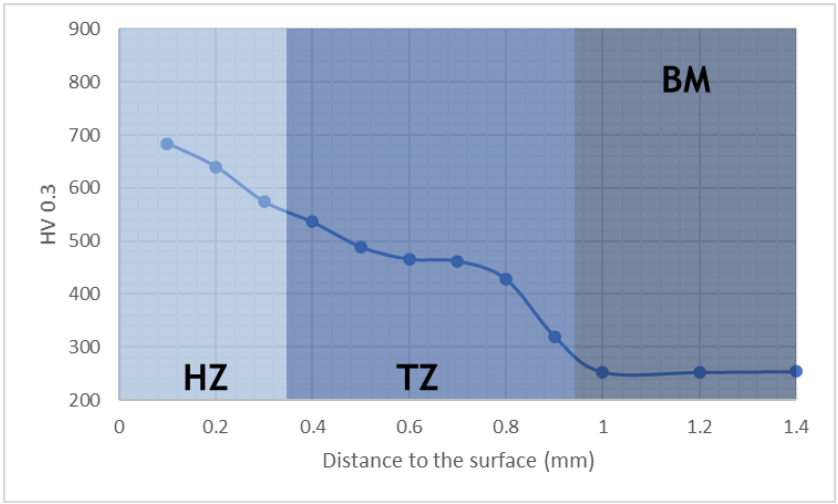

Specimen A3

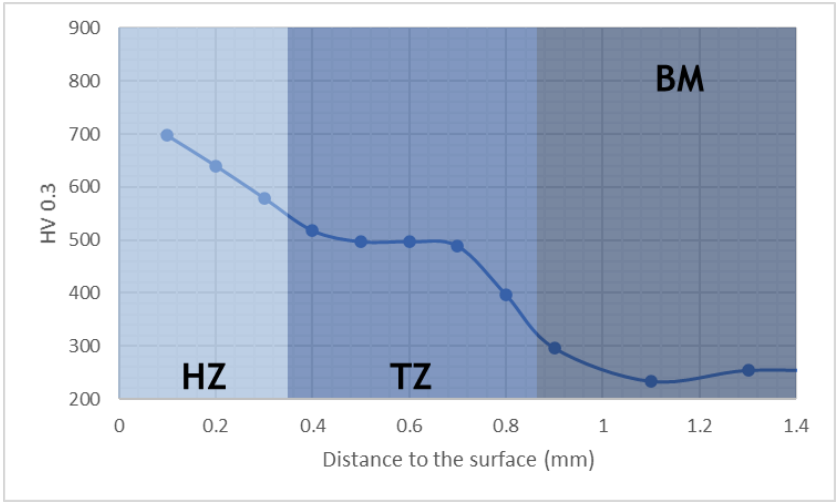

Specimen A4

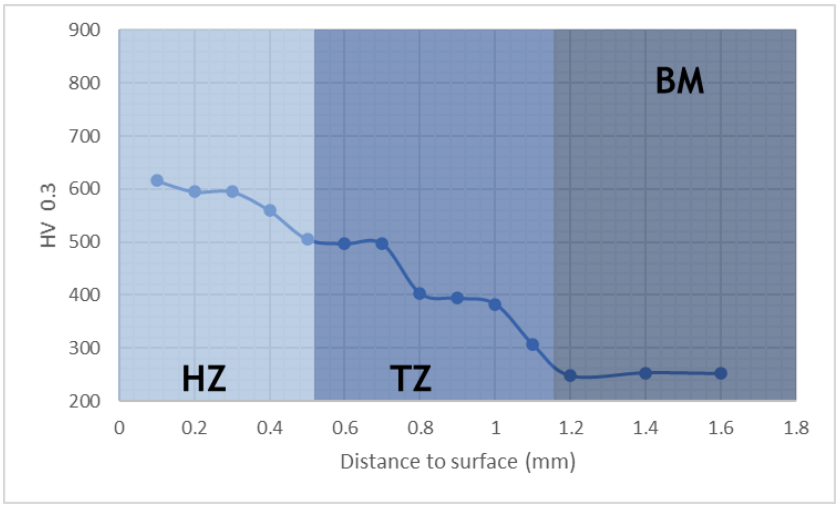

Specimen A5

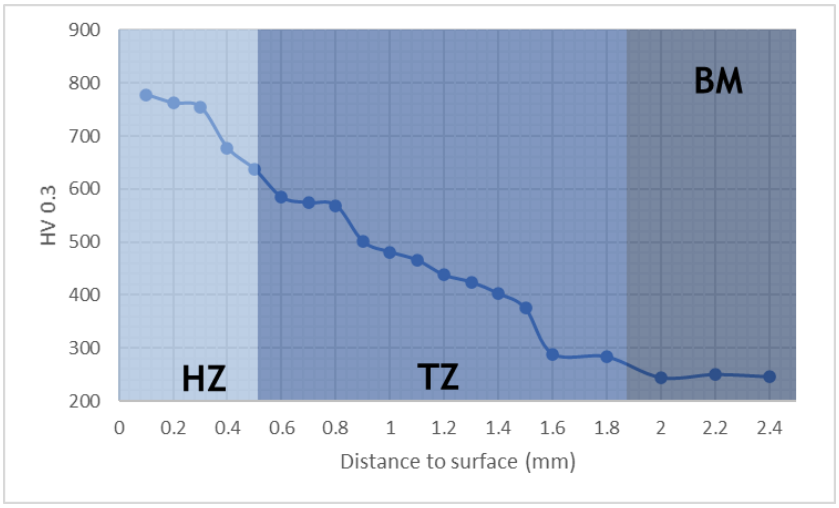

Specimen B1

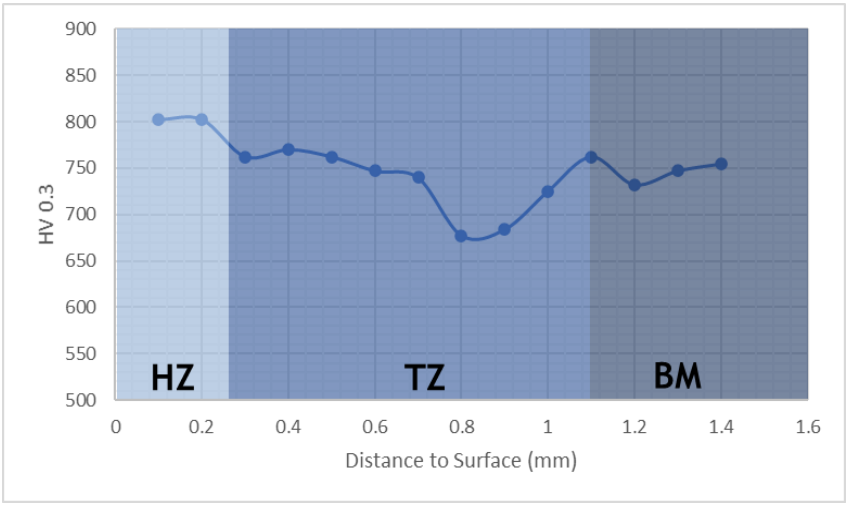

Specimen B2

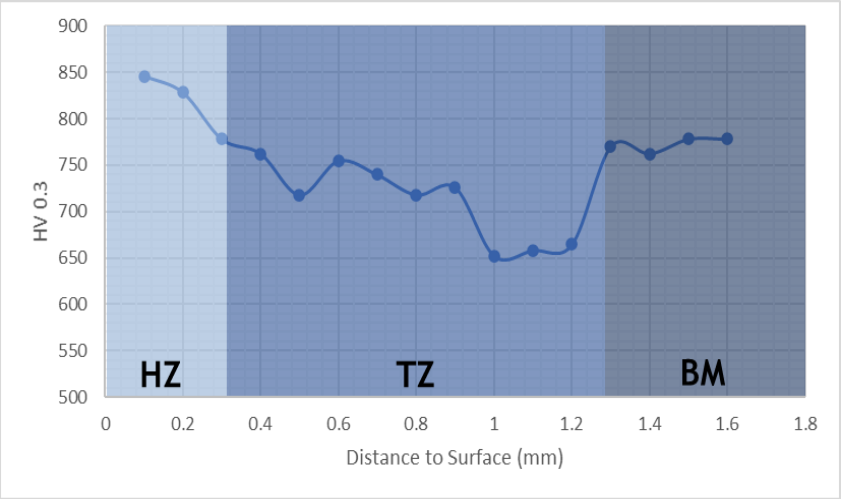

Specimen B3

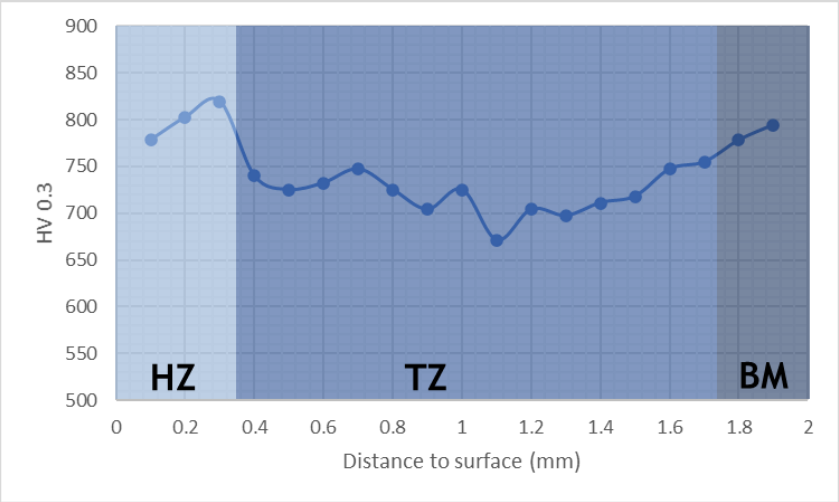

Specimen B4

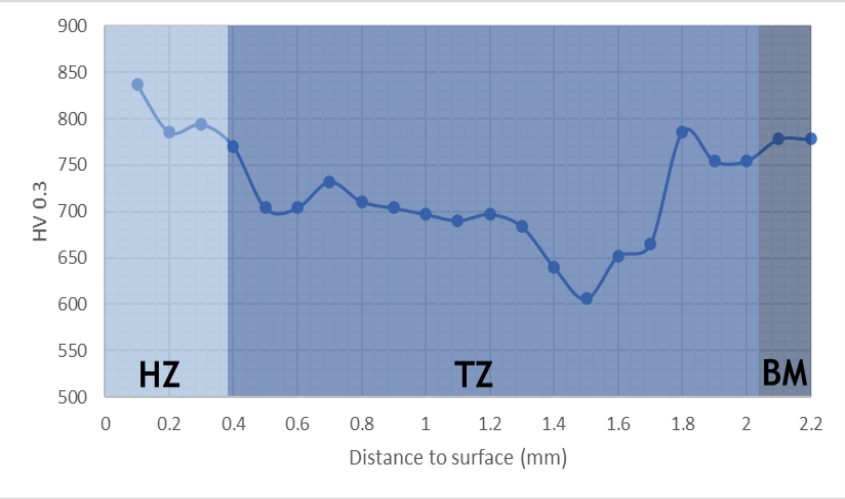

Specimen B6

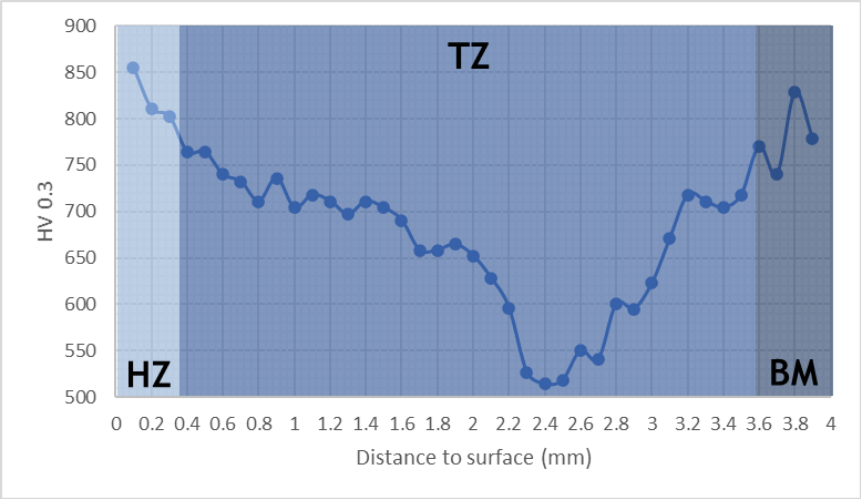
900
850
800
750
700
650
600
550
500
HV 0.3
TZ
HZ
BM
0 0.2 0.4 0.6 0.8 1 1.2 1.4 1.6 1.8 2 2.2 2.4 2.6 2.8 3 3.2 3.4 3.6 3.8 4
Distance to surface (mm)

III. XRD Analysis

Specimen A0

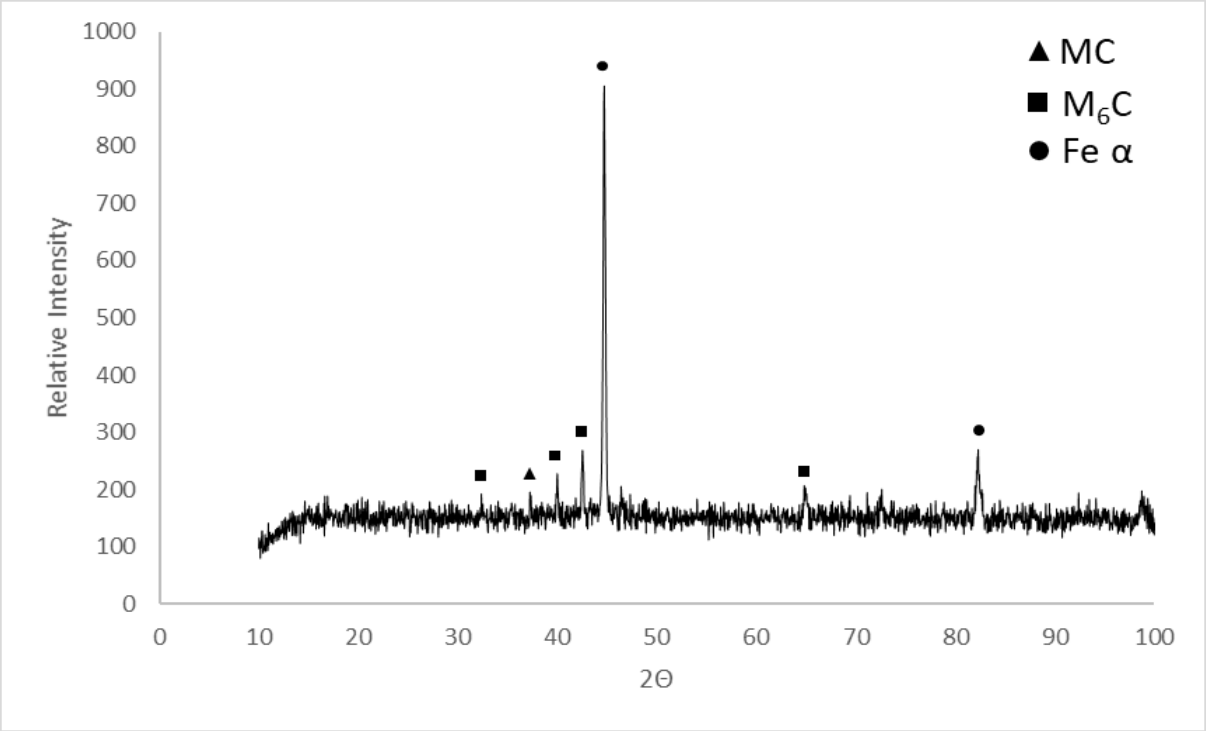

Specimen A6 – Hardened Zone

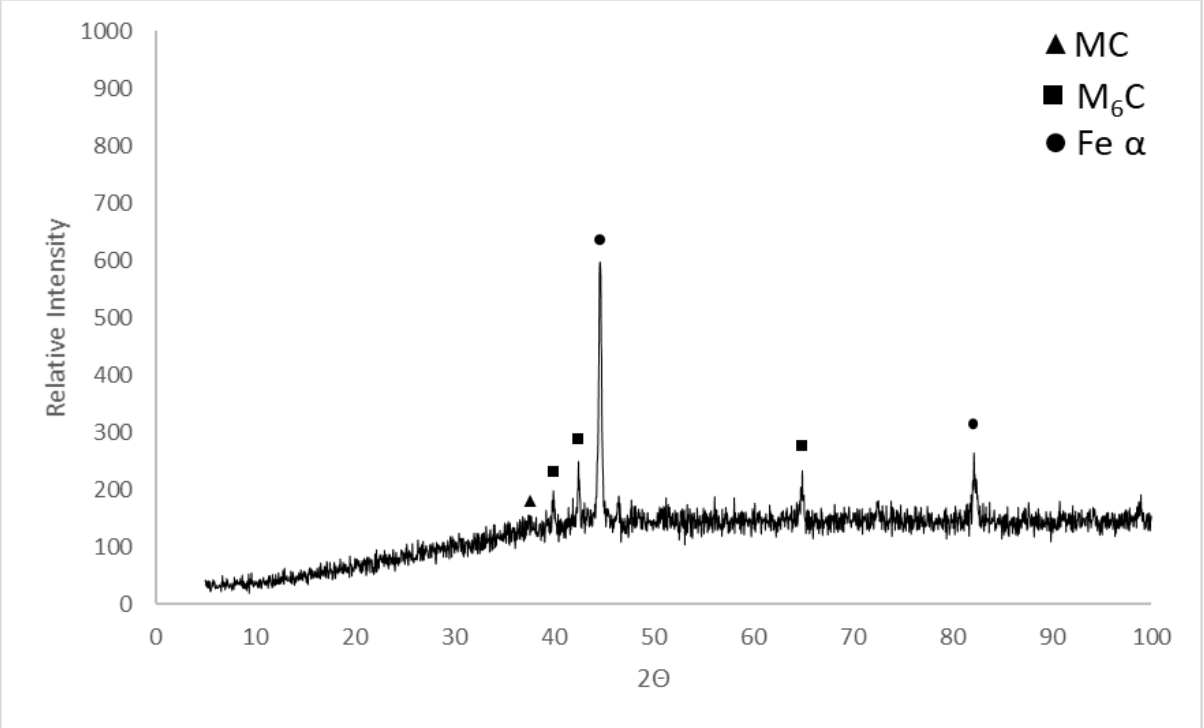

Specimen B0

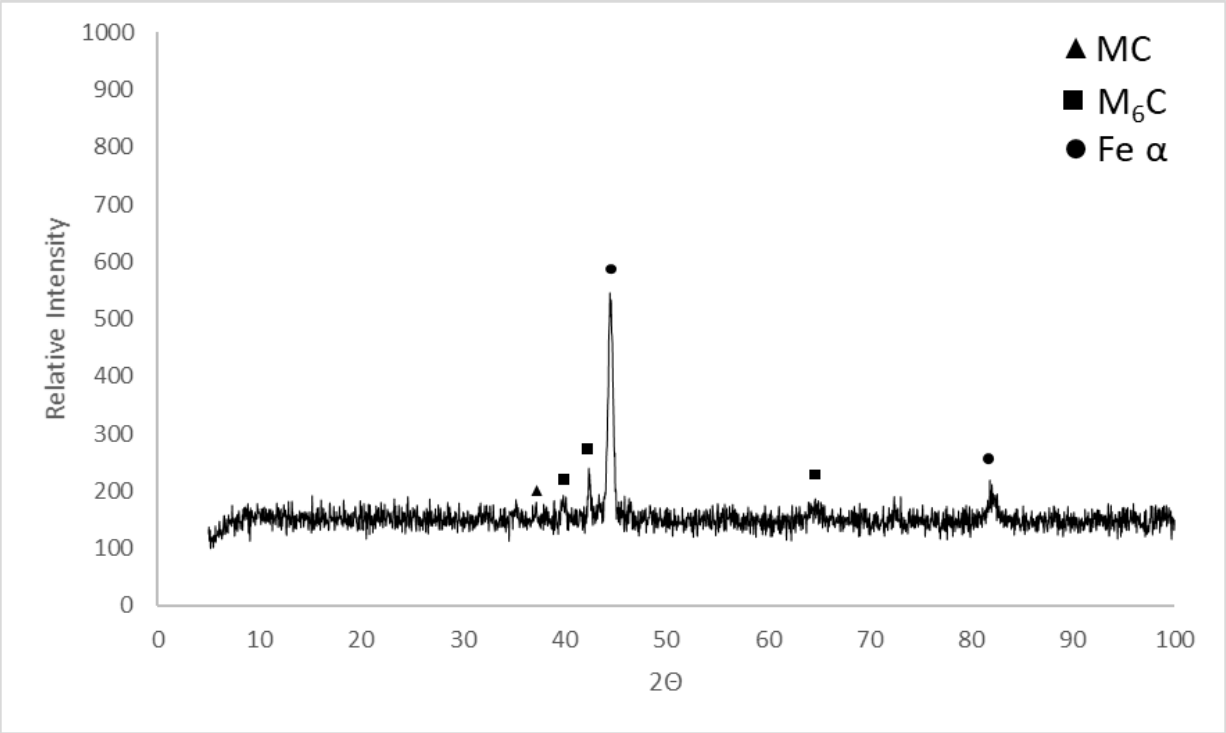

Specimen B5 – Hardened Zone

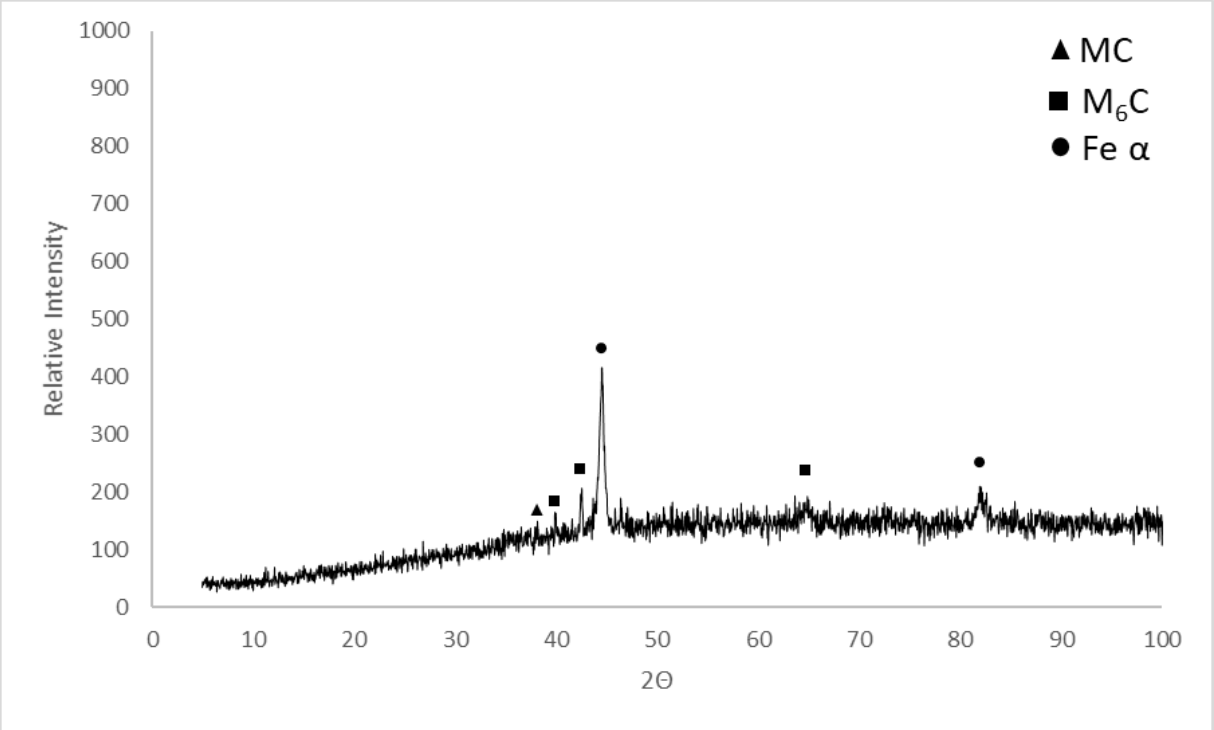

Note: ICCD cards 1-1159, 3-0980, and 11-0680 and bibliographic data [36, 44, 48, 65] were employed during the XRD analysis.